Construction and Building Materials 539 (2026) 147389

Contents lists available at ScienceDirect

Construction and Building Materials

journal homepage: www.elsevier.com/locate/conbuildmat

Strengthening of RC dapped-end beams with post-installed diagonal bars

Giovanni Menichini, Federico Gusella, Salvatore Giacomo Morano, Maurizio Orlando *

University of Florence, Department of Civil and Environmental Engineering, via di S. Marta, 3, Firenze 50139, Italy

ARTICLE INFO

Keywords:
RC structures
Dapped-end beams
Half-joints
Strengthening
Experimental tests

ABSTRACT

Dapped-end beams are critical regions in reinforced concrete (RC) bridges, since they can exhibit a brittle failure mechanism and are prone to deterioration. This study investigates the effectiveness of a post-installed internal diagonal steel bar as a strengthening solution for RC half-joints. Three specimens, one undamaged and two pre-damaged, were strengthened by embedding an M18 threaded bar in a 45° drilled hole filled with epoxy resin. Experimental results show that the strengthening method significantly increases the ultimate load and modifies the failure mechanism. The ultimate load increased by 61% for specimens without diagonal bars (type T1) and 34–40% for specimens with diagonal reinforcement (type T2), with crack widths reduced by up to 60% at service load levels. Strengthened specimens showed a change from localised splitting at the re-entrant corner to a more distributed diagonal cracking pattern. The study discusses the underlying load-transfer mechanism through a strut-and-tie interpretation and outlines practical application in existing bridge structures.

1. Introduction

Dapped-end beams in existing Reinforced Concrete (RC) bridges represent critical elements as declared by the 2020 Italian Guidelines [1], because they promote the accumulation of external deteriorating agents in addition to being difficult to inspect. Deterioration can compromise their load-bearing capacity and, in turn, that of the bridge itself as observed in recent collapses [2,3]. In many cases, a repair or retrofitting intervention is necessary. Moreover, existing bridges were designed according to outdated regulations that considered traffic loads lower than those prescribed by current standards, which could involve the need for strengthening interventions. In the context of intervention techniques on half-joints of existing RC bridges, the following strategies can be identified [4]:

1. Techniques aimed at modifying the load transfer mechanism to reduce or even eliminate the forces that existing half-joints must withstand, thereby enhancing safety even in the presence of damaged or deteriorated half-joints.
2. Repair or strengthen half-joints to restore or increase the load-bearing capacity, i.e., increasing the maximum force that the half-joint can transfer between the two deck segments by installing strengthening elements.
3. The closure of the half-joints.

Techniques of the first point include the temporary propping of the deck, as well as the installation of steel supporting elements, such as those used in the Acheregg Bridge near Stansstad, Switzerland [5]. A half-joint located near a pier can be unloaded using a steel support directly connected to the pier, as adopted in [6] for the helical ramp of the Polcevera Viaduct in Genoa. In [7], external post-tensioned cables have been installed to unload half-joints of a bridge in Japan. The replacement of end bearings with continuous bearings to improve load distribution at half-joints in two bridges on Haulbowline Island has been proposed in [8].

Concerning the second point, the strengthening systems for half-joints in existing bridges can be categorised as follows [4,9]: a) demolition and reconstruction of the half-joint while maintaining the same structural scheme, b) external or internal installation of ordinary or post-tensioned bars, c) external plating.

The demolition followed by reconstruction, even using innovative materials such as stainless-steel bars, high-performance concrete, and/or fibre-reinforced concrete, represents the simplest method for strengthening existing half-joints. However, this intervention is quite complex and costly. An example is represented by the strengthening project of the M2 motorway bridge over the River Medway in Kent, UK [10], where the central RC spans were replaced by steel beams, and half-joints were demolished and reconstructed.

Structural strengthening of half-joints in RC bridges can also be

* Corresponding author.
E-mail addresses: giovanni.menichini@unifi.it (G. Menichini), federico.gusella@unifi.it (F. Gusella), salvatoregiacomo.morano@unifi.it (S.G. Morano), maurizio.orlando@unifi.it (M. Orlando).

https://doi.org/10.1016/j.conbuildmat.2026.147389
Received 27 April 2026; Received in revised form 18 June 2026; Accepted 7 July 2026
Available online 20 July 2026

performed through the installation of ordinary or post-tensioned steel bars. The effectiveness of this methodology has been demonstrated in various interventions on existing bridges, such as the application on the Scafa Bridge in Fiumicino [11], or the intervention on the bridge over the Po River near Pieve Porto Morone [12], also investigated though numerical analysis in [13]. In [14], the strengthening of half-joints of a bridge over the Arno River has been performed through the post-installation of internal diagonal bars, while in [15], the effectiveness of the external prestressing technique has been investigated through an experimental campaign on seven RC half-joints. The near-surface-mounted technique for strengthening half-joints [16] involves inserting steel bars into grooves made on the concrete surface, which are then filled with epoxy resin to ensure force transfer. The failure of beams strengthened with this technique always occurred due to the sliding of the bars caused by a reduced anchorage length. In [17], an experimental campaign on half-joints has been conducted, proposing two strengthening techniques using steel bars: the first (ESA - Externally Strengthened Angles) involves applying steel angle brackets glued with epoxy resin, the second (USB - Unbonded Steel Bolt), uses threaded steel bars, inserted diagonally through holes inclined at 45°, which limit crack opening and increase beam ductility. For bridge decks with half-joints isolated or connected by a crossbeam placed behind the nib, the external jacketing technique can be utilized. In [17], an experimental campaign on external steel jacketing bonded with epoxy resin was conducted, showing resistance increases of 25–36% compared to unstrengthened specimens. External jacketing with steel plates connected to the existing concrete through bolted bars was also adopted in the strengthening of the Generale Franco Romano viaduct in Piemonte (Italy) along the A6 Highway [18,19].

In recent years, several studies have investigated the use of advanced composite materials to enhance the structural performance of reinforced concrete (RC) members. For instance, the study presented in [20] examined the shear behaviour of RC beams strengthened with a Fiber-Reinforced Geopolymer Matrix (FRGM) system consisting of small-diameter FRP bars embedded in a geopolymer matrix, highlighting the potential of this solution to improve both the strength and deformability of strengthened elements. Similarly, the study in [21] investigated hybrid beams made of Engineering Cementitious Composite (ECC) and reinforced with longitudinal Steel–FRP Composite Bars (SFCBs) together with FRP stirrups. The results demonstrated excellent structural and durability performance in aggressive environments, suggesting the suitability of these systems for marine and coastal engineering applications. Furthermore, the enhancement of the seismic performance of RC discontinuity regions through the application of Textile Reinforced Mortar (TRM) systems was investigated in [22], confirming the effectiveness of this strengthening technique. Finally, experimental campaigns reported in [23] and [24] focused on the behaviour of RC discontinuity regions strengthened with Carbon Fiber-Reinforced Polymer (CFRP) strips, providing valuable insights into the resisting mechanisms and effectiveness of CFRP-based strengthening interventions.

The first applications of fibre-reinforced polymers (FRP) for the external strengthening of half-joints were proposed in [17,25,26]. Nagy-György et al. in [27] conducted a series of tests on RC roof dapped-end beams, considering three different solutions with various fibre orientations. In [28], both experimental and numerical analyses on RC half-joints were conducted. After initial damage, the beams were strengthened using CFRP in three configurations: a single layer of horizontal fibres, a double layer of horizontal fibres, and crossed fibres, with the crossed-fibre arrangement proving to be the most effective. Sas et al. conducted a numerical study [29] to examine the effectiveness of combining techniques. In [30], Shakir and Abd analysed the behaviour of high-strength RC half-joints, strengthened with CFRP in different configurations. Abdelmoniem et al. [31] conducted a numerical analysis, calibrated with the experimental results of Taher [17], to examine the structural behaviour of half-joints strengthened with various techniques. Another external jacketing technique involves the use of Fibre Reinforced Cementitious Matrix (FRCM) composites, which combine the durability of cementitious mortars with the strength and lightweight properties of strengthening fibres. An experimental study has been conducted at the Polytechnic University of Milan by Flores Ferreira et al. [32], who examined three different strengthening configurations with FRCM to evaluate the influence of fibre orientation (0°, 45°, 0°+45°) in addition to the strengthening thickness. Baraghith et al. [33] proposed a particular strengthening technique based on the use of prefabricated plates made from Strain-Hardening Cementitious Composite (SHCC), which were studied in an experimental campaign; the proposed technique appears to be difficult to apply in common practice.

Finally, concerning the third point, when the strengthening of existing half-joints is not feasible, an alternative is represented by their closure, which also modifies the bridge's structural scheme. This approach has been documented in [5] regarding the bridge over the Seez River in Flums (Switzerland) as well as in [6]. In the end, it's worth recalling that while simplified analytical approaches, such as the strut-and-tie method, are commonly employed for the design and verification of dapped-end beams, recent advancements in computational modelling provide a more comprehensive understanding of their complex stress distributions and failure mechanisms [34].

1.1. Aim of the work

This paper presents the results of an experimental campaign carried out at the Structures and Materials Testing Laboratory of the Department of Civil and Environmental Engineering of the University of Florence. The experimental programme was divided into two parts. The first part, reported in a companion paper [35], investigated the failure behaviour of undamaged dapped ends with three different reinforcement layouts (T1, T2, and T3) considered representative of the most common configurations encountered in existing Italian small- to medium-span bridge decks.

The second part, presented in this paper, focuses on the behaviour of dapped ends strengthened by means of a post-installed diagonal steel bar. The strengthened specimens have the same geometry, materials, and reinforcement layouts as types T1 and T2 investigated in the first part of the research.

The strengthening was applied to both initially undamaged specimens and specimens intentionally pre-damaged prior to strengthening, allowing evaluation of the proposed technique under different initial conditions.

The strengthening system consisted of a post-installed diagonal steel bar, anchored at the top with a nut and bonded to the concrete along its anchorage length at the opposite end. This configuration reflects practical applications where bottom anchorage is often prevented by existing longitudinal reinforcement. The solution is particularly suitable for dapped-end beams connected by crossbeams, where external strengthening techniques are not feasible. However, its implementation requires sufficient internal space and drilling accessibility; therefore, T3 specimens were excluded due to severe reinforcement congestion. The effectiveness of the proposed strengthening technique is assessed through comparison with the results obtained for unstrengthened specimens reported in [35].

The paper is organised as follows. Firstly, the geometrical characteristics and structural details of specimens are described together with the geometrical and mechanical characteristics of the strengthening bar and the installation technique. Then the test setup, loading protocol and mechanical properties of the materials are presented; in the subsequent section, results are reported for each tested dapped end. Finally, the discussion of results highlights the impact of the proposed strengthening technique on the structural behaviour of half-joints, with particular focus on crack patterns up to failure and load-carrying capacity.

2. Experimental campaign

2.1. Reinforcement layout and strengthening configuration

Two types of strengthened full-scale RC half-joints (T1 and T2) were tested. Unstrengthened specimens of the same types had previously been tested up to failure in the first part of the research, with results reported in the companion paper [35]. The first part also included tests on specimens with a third reinforcement layout, named T3, characterized by the presence of multiple layers of diagonal bars, which did not allow the application of the proposed strengthening technique to T3 specimens. Therefore, the present study is limited to strengthened specimens of types T1 and T2.

The strengthening technique involves the post-installation of an 18 mm diameter threaded diagonal bar, inclined at 45°, embedded in a 22 mm diameter hole filled with epoxy resin. The total embedded length is 750 mm, with the bottom end positioned just above the bottom reinforcement bars. The geometry and reinforcement layout are shown in Fig. 1. The choice of an 18 mm diameter for the post-installed diagonal bar was guided by practical geometric constraints of the dapped-end region. Smaller diameters would have provided a limited contribution in terms of additional tensile area, while larger diameters would require drill holes that may interfere with existing reinforcement or reduce the residual concrete section around the re-entrant corner.

In specimen T1–1B, the bottom longitudinal reinforcement bars were welded to a steel end anchorage plate to prevent the slippage phenomenon noticed in the earlier phase of the experimental program described in [35]. Besides the vertical stirrups at 75 mm spacing, in specimen T1–1B, there are two 16 mm horizontal U bars; in T2 specimens, there are two 8 mm horizontal U-bars and a pair of 12 mm diagonal bars (Fig. 1), whose top ends are intentionally misaligned with the nib support, as usually found in existing half-joints. In all specimens, there are two vertical 14 mm bars and the first stirrup is always positioned 120 mm from them to account for the potential presence of a cross beam (dashed area in Fig. 1). The two chosen layouts resemble those of existing Italian bridges [3,36].

Two beams for each dapped-end type have been cast for a total of eight dapped ends; then, each dapped end has been labelled as follows: Tα-βΔ-Ω, where: α= 1, 2 denotes the type (T1 or T2); β= 1, 2 denotes the absence (1) or presence (2) of strain gauges on rebars; Δ=A, B distinguishes the two dapped ends of the same specimen (left side or right side) and Ω=D or S, where D denotes pre-damaged and S strengthened specimens.

2.2. Specimen dimensions and test setup

Each dapped-end beam has an overall length of 4120 mm and a full-depth rectangular cross-section measuring 250 × 600 mm² (Fig. 2). The nib extends 200 mm in length and has a depth of 300 mm, which is half the total depth of the beam. To prevent flexural failure, the flexural reinforcements are oversized. Shear reinforcement consists of 8 mm vertical stirrups, arranged at two different spacings: 75 mm near the dapped end and 150 mm further away. Each specimen was subjected to a three-point asymmetric bending test under simply supported

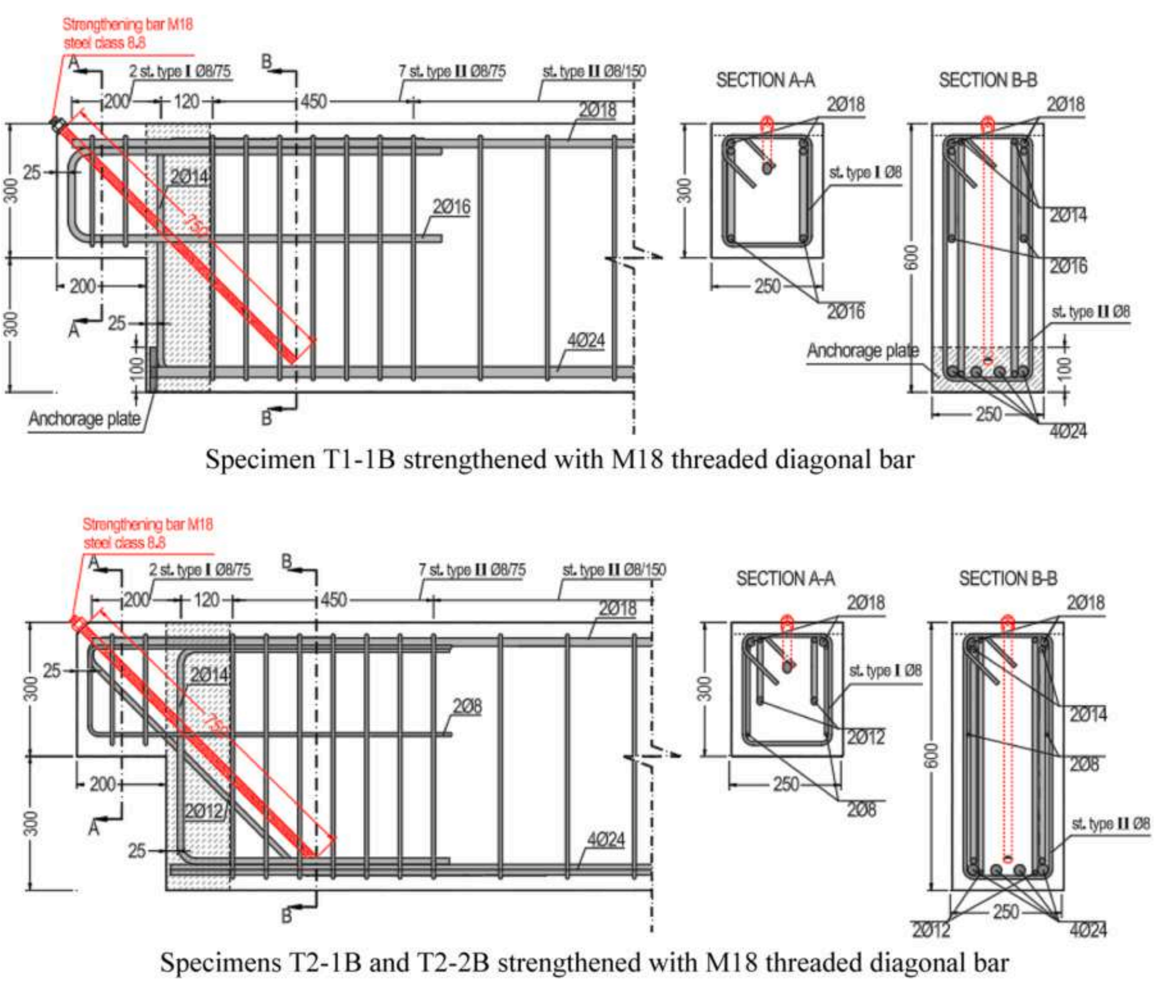

Fig. 1. Geometry and reinforcement layout of the two dapped end types (the dashed area identifies the potential presence of a cross beam) with the post-installed diagonal bar.

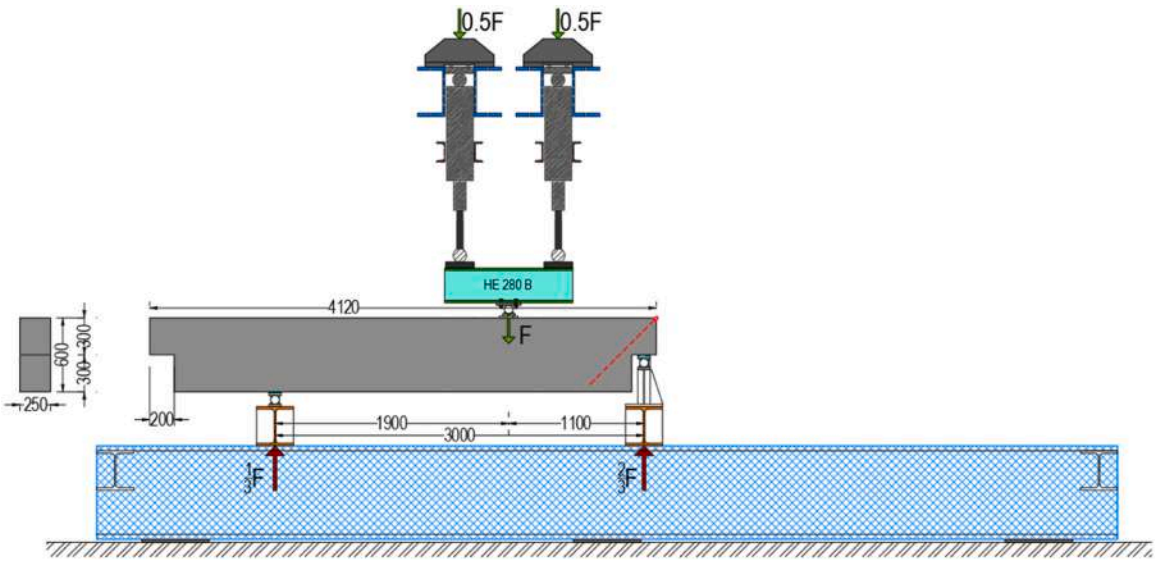

Fig. 2. Three-point non-symmetric bending test with the identification of the reactions at external supports [mm] [35].

conditions, with an effective span of 3000 mm (Fig. 2). The vertical load is applied 1100 mm from the support of the tested dapped end (approximately one-third of the effective span), using two electromechanical actuators, each with a maximum load capacity of 350 kN, which provide a total load capacity of 700 kN.

The distance of 1100 mm between the applied load and the vertical support beneath the nib corresponds to twice the effective depth of the beam (550 mm), avoiding the formation of a direct concrete strut to the support, as recommended in [11,12,26,31]. The applied force, F, is transferred to the specimen through a rigid steel beam (HE 280 B) (Fig. 2). Both supports, one located at the beam bottom and the other at the tested dapped end, consist of welded steel cylinders with a 50 mm diameter. The reactions at the supports are distributed as 11 F/30 (about F/3) beneath the beam end and 19 F/30 (about 2 F/3) beneath the dapped end.

The loading protocol consisted of a monotonic load applied up to failure under displacement-controlled conditions. However, to evaluate the effectiveness of the proposed technique on damaged dapped ends, some specimens were pre-damaged before being strengthened.

The pre-damage protocol involved applying increasing loading steps until reaching a peak load equal to approximately 98% of the ultimate capacity of the corresponding unstrengthened reference specimen. This stepped procedure allowed for a controlled accumulation of damage and cracking, while preventing premature sudden failure.

After completion of the pre-damage phase, the specimens were unloaded, strengthened with the post-installed diagonal steel bar, and subsequently tested to failure. Pre-damage was induced by loading the specimens using the same configuration adopted for the final failure tests, ensuring that cracking and steel yielding developed along the same load paths. The high threshold (98%) was deliberately selected to simulate a severe near-collapse condition, representative of a worst-case scenario for existing bridges. This approach enables a rigorous assessment of the strengthening system and its effectiveness in restoring the load-bearing capacity, even in the presence of extensive damage.

2.3. Strengthening of specimens

To install the strengthening diagonal bar, preliminarily, the top edge of the dapped end was smoothed at 45°, then a 22 mm diameter hole was drilled into the dapped end with the help of a steel custom-made jig, designed to ensure accurate positioning of the hole and 45° inclination. The hole was then thoroughly cleaned, initially using compressed air to remove dust and debris, then washed with clean water, and residual moisture was removed by vacuum extraction. Finally, the hole was filled with epoxy resin, and the threaded bar was embedded, as shown in Fig. 3, and anchored externally with a nut and a 50 mm diameter washer.

The adopted strengthening solution (a diagonal bar with a diameter of 18 mm) may be particularly suitable in the presence of crossbeams, which can prevent the installation of external strengthening bars on either side of the dapped end, as can be done for isolated dapped ends. However, the use of internally embedded strengthening bars is feasible only when sufficient internal space is available and drilling operations are not hindered, as in the case of the T3 specimens, which were excluded from strengthening due to their extremely high reinforcement density. It is worth noting that an 18 mm bar diameter, with a 22 mm drilled hole, was considered the minimum feasible size to avoid drilling tool failure and drilling misalignment. At the same time, this diameter was selected to ensure that the load-carrying capacity of the strengthened specimens remained within the capacity limits of the laboratory testing equipment.

Regarding the long-term durability of the strengthening technique, the epoxy resin utilized in this research is certified in the ETA−22/0001 [37] for a service life of at least 100 years within a wide temperature range of −40°C to + 72°C. These performance values are valid when the system is installed in compacted, non-carbonated concrete, respecting a minimum concrete cover provided in [37]. This configuration also benefits from a "reserve length" effect [38]: while the outermost segment of the bar-concrete interface might experience minor environmental degradation, the deep internal segment remains shielded, ensuring the load transfer capacity is maintained.

2.4. Specimen material properties

All specimens were constructed using concrete of grade C25/30 (f_{ck}=25 N/mm^2) and steel rebars of grade B450C (f_{yk}=450 N/mm^2). The compressive strength of concrete had been assessed through five uniaxial compression tests on cylinder specimens (diameter x length = d x L ≈ 100 mm×190 mm) according to EN 12390–3 [39] at testing ages between 96 and 272 days. All tests provided remarkably similar values of the cylinder compressive strength with an average value f_c ≈ 40.4 N/mm^2 and a standard deviation of 3.1 N/mm^2. The concrete compressive strength has also been evaluated at a testing age of 320 days through compression tests on twenty-three core specimens drilled from beams after completing tests on dapped ends. Results allow for estimating an average cylinder compressive strength f_c ≈ 40 N/mm^2 with a

Fig. 3. Execution phases for the installation of the diagonal strengthening bar.

standard deviation of 3 N/mm^2 (COV=0.075), which is remarkably similar to values from initial characterization compression tests. The tensile strength is evaluated through five splitting tensile tests, according to EN 12390–6 [40]. The average splitting tensile strength (f_{ct}) is 4.27 N/mm^2 with a standard deviation of 0.58 N/mm^2. The elastic modulus of the concrete holds 29045 N/mm^2 and is evaluated according to EN 12390–13 [41].

The steel reinforcement consists of ribbed bars with a nominal yield strength of 450 MPa and a ductility grade C (B 450 C). Uniaxial tensile tests provided average values of the yield strength (f_y) between 498 N/mm^2 (8 mm bars) and 548 N/mm^2 (12 mm bars) and values of the ultimate strength (f_u) between 602 N/mm^2 (8 mm bars) and 655 N/mm^2 (12 mm bars). The results of all compression tests on concrete specimens and tensile tests on steel rebars have already been reported in [28]. Two additional uniaxial tensile tests were performed on 18 mm threaded bar specimens, yielding average values of 664 MPa for yield stress and 801 MPa for ultimate stress, with coefficients of variation of 0.63% and 0.7%, respectively. The 18 mm threaded steel bars were anchored in 22 mm diameter holes in cracked concrete. According to the European Technical Assessment ETA-22/0001 [37], the characteristic bond resistance in uncracked concrete C20/25 for reinforcing bars in hammer drilled holes is 14 MPa, referred to the lateral surface of the bar.

2.5. Specimen Instrumentation

The specimens were subjected to displacement-controlled loading at a constant stroke rate of 1 mm/min and were monotonically loaded beyond the peak load. The structural response of the dapped ends is monitored using instruments placed on both the right and left faces along the main reinforcement bars (Fig. 4). To measure crack opening displacements, linear variable differential transformers with a resolution of ±0.01 mm (LVDTs) are installed on all specimens in various directions: diagonal (LVDT5, LVDT10, LVDT11, LVDT6), horizontal (LVDT2, LVDT7), and vertical (LVDT3, LVDT8). The distances between the instrumented points are indicated in Fig. 4, which also shows the exact positioning of all LVDTs.

Three wire encoders (F1, F2 and F3) are fixed to the ground to measure the vertical displacement at the target point (d_{F2}), located at the bottom of the loaded section, and the vertical displacements at the supports (d_{F1} and d_{F3}); the last have been removed from the recorded value of $d_{F2,}$ according to the procedure described in [35], to account for the deformability of the loading frame. Instrument data acquisition was performed at 10 Hz. Strain gauges were installed on the stirrups near the nib, and their position was depicted in [35].

3. Experimental tests

3.1. Experimental program

The experimental campaign was conducted on three dapped-end specimens, all of which were first strengthened and then tested to failure; however, the strengthening was applied under different initial conditions for the specimens. In the first investigated case, the strengthening was applied to the undamaged specimen T2–1B, that is, to

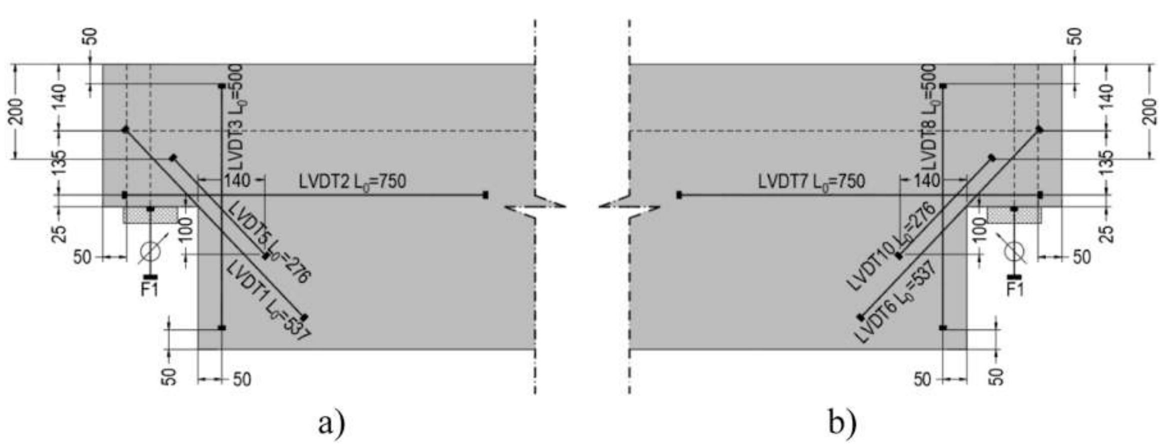

Fig. 4. Identification of the length and position of the linear variable differential transducers (LVDTs) a) Front face b) Backside face.

the specimen in its original as-built condition with no prior loading history. In the other two cases (specimens T2–2B and T1–1B), the strengthening was applied to specimens that had been pre-damaged through a stepwise loading and unloading process, up to reach about the same ultimate load recorded during the failure tests conducted in the first part of the study. The pre-damage procedure used for specimens T2–2B and T1–1B is non-standardised. It involved a series of random, load-controlled cycles up to 98% of the ultimate load previously recorded for homologous specimens in the previous experimental campaign [35]. Stabilization intervals of 60–90 s were incorporated to allow crack stabilization. This protocol ensured a consistent level of damage representative of in-service deterioration in dapped-end beams.

3.2. Test results

3.2.1. Specimen T2−1B

The undamaged specimen T2–1B is first strengthened with the diagonal 18 mm threaded bar and then tested to failure (test T2–1B-S). The strengthened specimen exhibited a 34.32% increase in load capacity compared to the unstrengthened specimen T2–1A, and a 39.66% increase compared to the unstrengthened specimen T2–2A. The load-displacement curve for the investigated specimen is compared with the unstrengthened specimen of the same typology, i.e. with the same reinforcement layout (Fig. 5). The crack pattern analysis provides a visual and qualitative understanding of how damage evolves in both unstrengthened and strengthened specimens (Fig. 10). By comparing the crack pattern at failure of the strengthened specimen T2–1B-S with the unstrengthened specimens T2–1A and T2–2A, a completely different failure mode is observed. In the unstrengthened specimens, no slippage of the bottom reinforcement bars had been observed [28], and the cracking had been primarily concentrated at the inner corner of the nib, propagating diagonally at an angle of approximately 45° up to the top concrete cover.

In the strengthened specimen, the addition of a threaded diagonal bar produced such an increase in the ultimate load that it caused a corresponding increase in the stresses of the bottom reinforcement bars, leading to their failure by bar slippage. A series of distributed cracks developed along the length of the bottom bars, eventually ending in a main crack with an inclined orientation (about 55°), extending through the entire height of the beam's full-depth section. It can be assumed that the presence of an anchorage plate at the end of the bottom bars could have contributed to an increase in the ultimate load. However, this

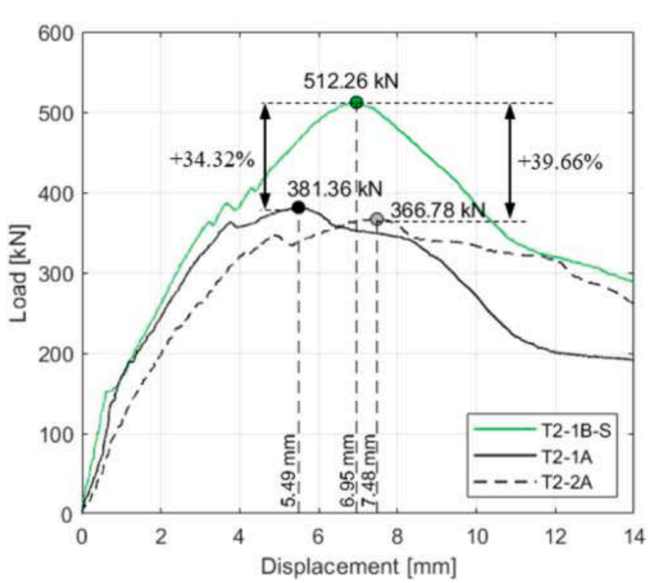

Fig. 5. Load-displacement curve of the test T2−1B-S and comparison with tests on unstrengthened specimens T2−1A and T2−2A.

hypothesis should be evaluated through further FEM modelling of the test, considering both the actual configuration and a modified configuration including an end plate. Concerning the crack width, Fig. 11 illustrates the evolution of crack opening displacement (COD) as a function of the applied load. In all measurement points, the COD increases nonlinearly with the load, with significant differences in both the rate and magnitude of crack opening between the unstrengthened and the strengthened specimens. The strengthened specimen T2–1B-S consistently exhibits the lowest COD values across all LVDT locations, even at loads approaching the ultimate value P_u. This behaviour indicates improved crack control due to the redistribution of internal stresses, due to the presence of the post-installed diagonal bar. The COD in T2–1B-S remains below approximately 2 mm throughout the loading process, confirming the effectiveness of the strengthening in limiting deformation and delaying damage accumulation.

In contrast, the unstrengthened specimens T2–1A and especially T2–2A show a much steeper increase in crack opening beyond 250–300 kN, with the latter reaching peak COD values of up to 6 mm, particularly at LVDT positions 1–6. These results reflect an earlier onset of cracking and a reduced capacity for crack diffusion in the absence of the strengthening bar. Among the four measurement points, LVDT pairs 1–6 and 5–10 display the largest crack openings and the most pronounced differences between the specimens, since these locations correspond to the most critical zones, where the strengthening bar has the greatest influence.

Although specimens T2–1A and T2–2A have the same reinforcement layout, their load–displacement curves exhibit moderate differences. Such variations are consistent with the expected scatter in full-scale reinforced concrete elements and may be attributed to local differences in initial micro-cracking, small variations in aggregate distribution near the dapped-end region, or minor geometric imperfections in the nib or the supporting boundary conditions. These differences fall within the typical variability observed in large-scale RC tests and do not affect the interpretation of the strengthening effectiveness.

3.2.2. Specimen T2−2B

Specimen T2–2B was first subjected to a pre-damage test under a stepwise loading and unloading process to reproduce the cracking state that might be produced by live loads in overloaded existing half-joints. Then, it was strengthened and tested to failure (Fig. 6). During the pre-damage test, the specimen was subjected to stepwise loading and unloading until a value close to the ultimate load reached in failure tests on as-built specimens with the same reinforcement layout (T2–1A and T2–2A in [35]). Subsequently, the pre-damaged specimen was strengthened using the diagonal 18 mm threaded bar, and finally, the monotonic failure test (T2–2B-S) was carried out.

Fig. 7 shows the loading protocol, defined by the displacement imposed by the hydraulic jacks, alongside the load-displacement curve. During the pre-damage test T2–2B-D, the first two loading steps, at 101.42 kN and 104.82 kN (corresponding to 26.6% and 27.4% of the ultimate load of the unstrengthened specimen T2–1A) resulted in the initiation of a hairline crack, slightly visible at the inner corner of the nib. Subsequently, the application of a 202.24 kN (52.9%) load caused the opening of a 0.2 mm-wide diagonal crack, at approximately 45°, originating from the same inner corner. After unloading, the specimen was reloaded up to 290.92 kN (76.2%). At this loading level, the diagonal crack widened to 0.6 mm. Upon unloading, the crack partially closed, maintaining a residual opening of 0.2 mm.

A further loading step up to 276.52 kN (72.4%) was then applied, during which the diagonal crack continued to propagate, reaching an opening of 0.67 mm. Once again, after unloading, the crack closed partially, with a residual width of 0.2 mm. A subsequent load step up to 363.70 kN (95.2%) caused the formation of a second diagonal crack, inclined at approximately 50°, originating from the edge of the bearing plate.

The final two loading steps were applied up to 366 kN (95.8%) and

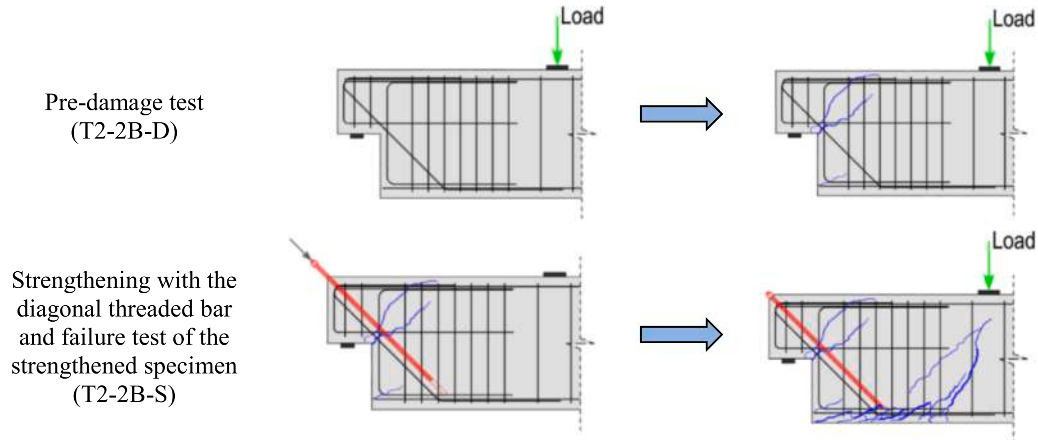

Fig. 6. Test phases of the specimen T2−2B.

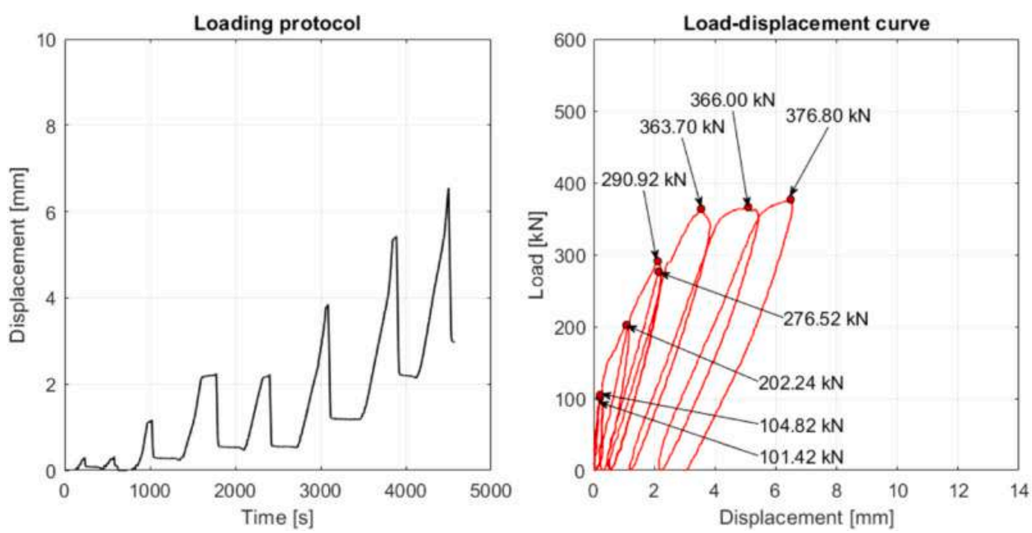

Fig. 7. Loading protocol and load-displacement curve for the pre-damage test T2−2B-D.

376.8 kN (98.7%), respectively. The last value of 376.8 kN was between the ultimate loads reached in the failure tests on specimens T2–1A and T2–2A (366 kN and 381 kN). During these phases, the diagonal cracks widened from 0.83 mm to 3.63 mm at the first peak and 5.31 mm at the second peak. After the final unloading, the residual total width of the two diagonal cracks was equal to 3.48 mm.

Fig. 8 illustrates the evolution of the crack opening displacement (COD) as a function of the applied load during the T2–2B-D damage test. The solid line represents the COD at the peak load of each loading step, while the dashed line indicates the residual crack opening measured after complete unloading. After the pre-damage test, the specimen was strengthened using the diagonal threaded bar, and then the failure test (T2–2B-S) was conducted. The load-displacement curve of T2–2B-S is compared with the unstrengthened specimen of the same typology (Fig. 9). The capacity curve of the strengthened specimen T2–2B-S highlights about the same increase in load capacity. Specifically, it exhibited a 28.86% increase in load capacity compared to the unstrengthened specimen T2–1A, and a 33.98% increase compared to T2–2A. By comparing the crack pattern at failure of the strengthened specimen T2–1B-S and T2–2B-S with the unstrengthened specimens T2–1A and T2–2A, a completely different failure mode is observed (Fig. 10). In the unstrengthened specimens, no slippage of the bottom reinforcement bars was observed, and cracks were primarily concentrated at the inner corner of the nib, propagating at an inclined angle of approximately 45° toward the top concrete cover. In the strengthened specimen, the installation of the diagonal bar led to increased stresses in the bottom reinforcement bars, causing their failure by slippage. In this case, a series of distributed cracks developed along the length of the bottom bars, culminating in a dominant inclined crack, approximately 60°, that extended through the entire height of the beam, resulting in a full-depth failure section.

Fig. 11 shows the evolution of crack opening displacement (COD) as a function of the applied load for specimen T2–2B-S. In the test, performed after strengthening with the diagonal threaded bar, COD values increased more gradually and remained lower at the maximum load P_u compared to the unstrengthened specimens T2–1A and T2–1B, indicating improved crack control and a more distributed damage pattern. It is important to note that curves of T2–1B-S do not start from zero, but from the residual values recorded at the end of the pre-damage test (T2–2B-D). The comparison confirms that the strengthening effectively reduced the damage state of the dapped end.

During the pre-damage test, the strain gauges SG1, SG2 and SG3 recorded increasing strains approaching or slightly exceeding the yield strain of the bars (notably SG2 and SG3). All three sensors ceased functioning near the yield strain due to damage.

Strain gauges SG4, SG5, and SG6, positioned on the first, second, and third stirrups, respectively, remained functional throughout the test, recording strains below the yield point. In the T2–2B-S test, SG4 exhibited a maximum strain approximately 20% lower than in T2–2B-D, indicating a significant difference. For SG5, the difference was smaller,

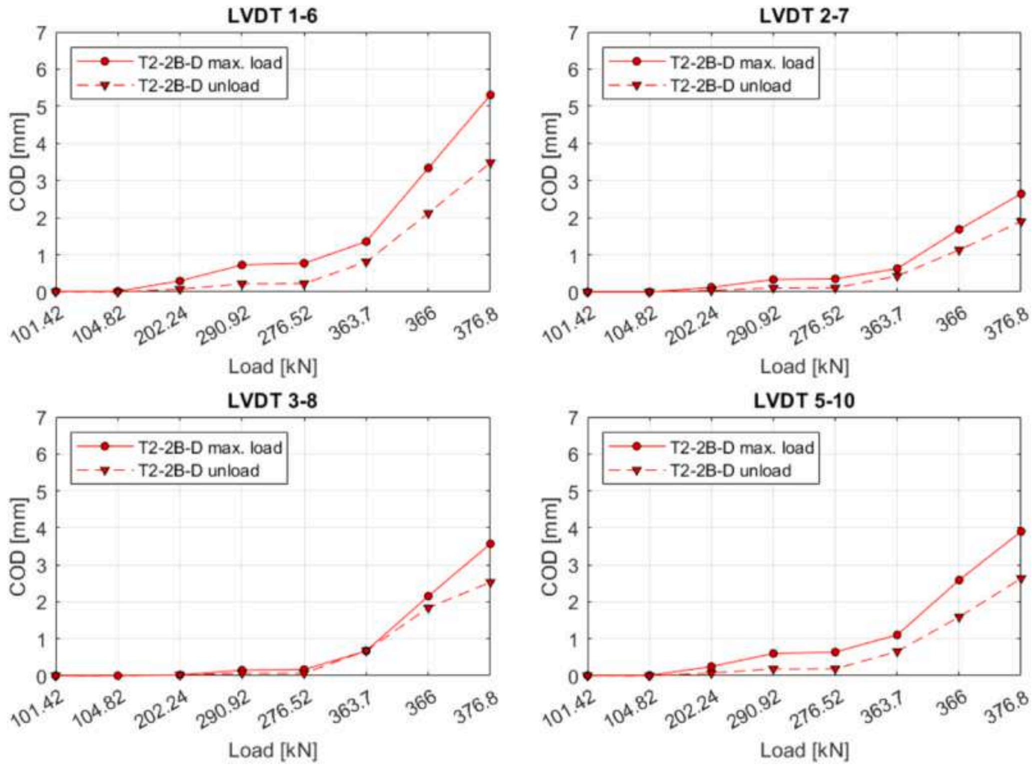

Fig. 8. Average crack opening displacements measured by all LVDTs as a function of the applied load (P) [kN] for the pre-damage test T2−2B-D.

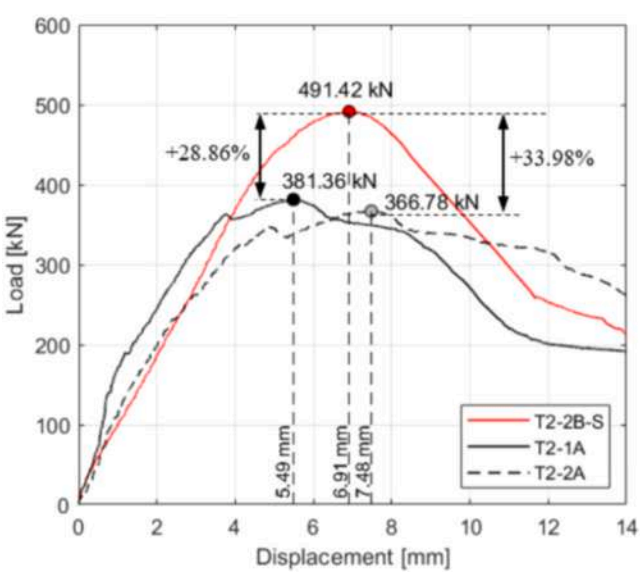

Fig. 9. Load-displacement curve of the test T2−2B-S and comparison with tests on unstrengthened specimens T2−1A and T2−2A.

with the maximum strain in T2–2B-S about 4% lower than in T2–2B-D. This reduction is attributable to the introduction of the diagonal reinforcement bar in T2–2B-S, which reduces the stress state in the stirrups. SG6 recorded only modest strain variations, suggesting that the third stirrup played a minimum role in the failure mechanism (Fig. 12).

3.2.3. Specimen T1−1B

Like specimen T2–2B, specimen T1–1B was first pre-damaged under a stepwise loading and unloading process. After the pre-damage test, the specimen was strengthened with the diagonal threaded bar and subjected to a new monotonic test to failure (test T1–1B-S) as depicted in Fig. 13.

Fig. 14 shows the loading protocol for the pre-damage test, along with the corresponding response of the tested specimen. The figure highlights the load levels attained during the test.

The pre-damage test was performed by initially applying a 101.14 kN (27.7%) load, followed by a complete unloading phase. No crack formation was detected during the initial stage. Successively, a load of 283.56 kN (77.6%) was applied, which led to the initiation of a hairline crack at the inner corner of the nib. All percentages refer to the maximum load of the unstrengthened specimen T1–2B.

This crack exhibited an inclination of about 45°, and its width progressively increased as the applied load increased. Following the unloading, the crack closed partially, maintaining a residual width of 0.5 mm. Ultimately, two additional loading increments were applied up to 324.40 kN (88.8%) and 342 kN (93.7%), after each of which the specimen was unloaded.

The pre-existing crack propagated in length and widened, but did not extend to the upper concrete cover. Partial crack closure was observed upon unloading, with a residual opening of about 1.0 mm. Fig. 15 illustrates the evolution of the crack opening displacement (COD) as a function of the applied load during the T1–1B-D damage test. The solid line represents the COD at the peak load of each loading step, while the dashed line indicates the residual crack opening measured after complete unloading.

After the pre-damage test, the specimen was strengthened with the diagonal threaded bar and then tested to failure (T1–1B-S). During the test, a hydraulic circuit issue caused an interruption at a load of approximately 539 kN. The specimen was subsequently reloaded, reaching an ultimate load of 587 kN. The load–displacement curve of the strengthened specimen (T1–1B-S) is compared with those of the unstrengthened specimens of the same type (T1–1A and T1–2B) in Fig. 16. The curves highlight clear differences in both peak load capacity and stiffness. The strengthened specimen exhibits the highest ultimate load, reaching 586.84 kN, and shows an intermediate peak of 538.58 kN during the unloading and reloading sequence before attaining its final

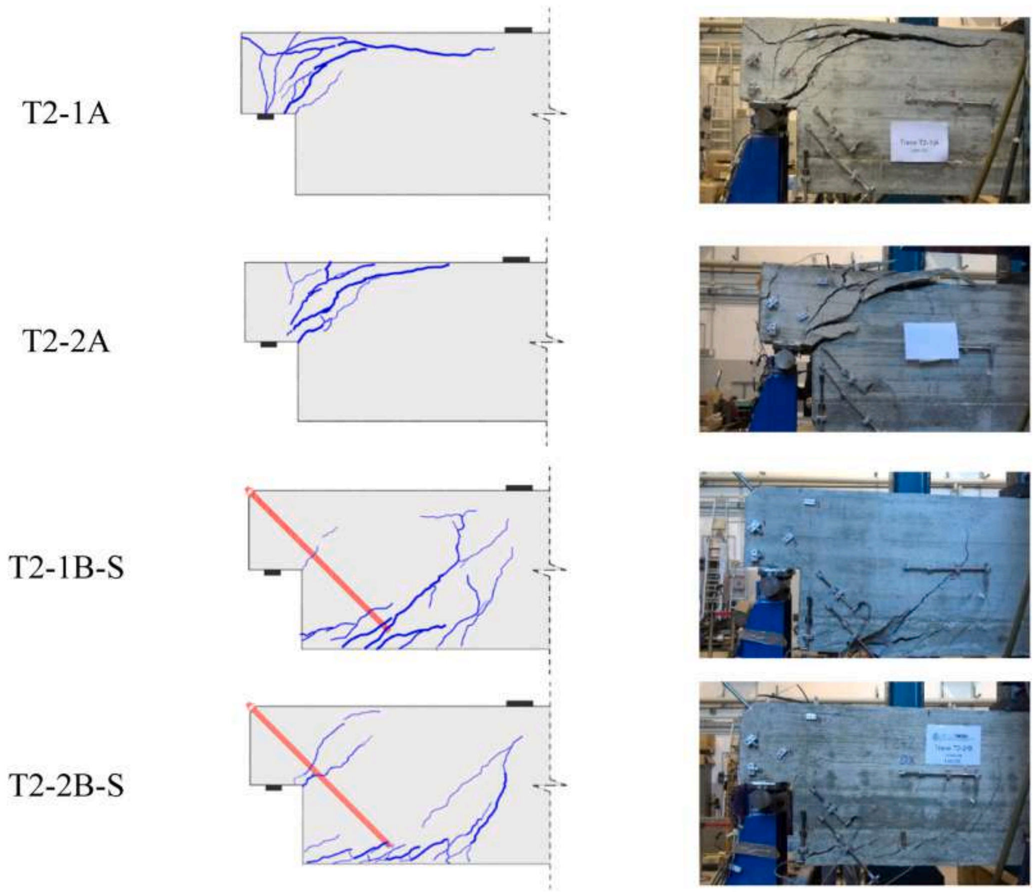

Fig. 10. Crack pattern at failure for tests T2−1B-S and T2−2B-S and comparison with unstrengthened specimens T2−1A and T2−2A [35].

capacity.

Compared to the unstrengthened specimens, T1–1B-S shows a 63.96% and 60.54% increase in peak load relative to T1–1A and T1–2B, respectively, demonstrating the effectiveness of the diagonal bar in enhancing structural performance.

The crack patterns at failure are compared in Fig. 17. In the strengthened specimen T1–1B-S, cracking is more distributed and finely developed, with multiple inclined cracks starting from the inner corner of the nib and propagating diagonally. In contrast, unstrengthened specimens T1–1A and T1–2B show more localized and wider diagonal cracks.

Fig. 18 illustrates the evolution of crack opening displacement (COD) with increasing applied load, measured at four LVDT positions (1–6, 2–7, 3–8, and 5–10). The curve for specimen T1–1B-S is shown over two steps (first and second loading phases), along with curves related to unstrengthened specimens T1–1A and T1–2B. The data show that during the first loading step of T1–1B-S, the COD remains consistently lower than in the unstrengthened specimens, indicating effective crack control and delayed damage development due to the presence of the diagonal bar. In the second step, COD values increase more rapidly - particularly at LVDT positions 1–6 and 3–8 - reflecting the influence of prior damage accumulated during the first step. Nevertheless, in positions such as LVDT 2–7 and 5–10, the COD values in the second step remain comparable to or even below those observed in the unstrengthened specimens. Overall, the comparison highlights the beneficial effect of the diagonal strengthening in reducing crack opening during the first loading step.

3.2.4. *Load-carrying capacities from all tests*

Table 1 summarizes the load-carrying capacities registered in all the failure tests, including those previously reported in [35]. The percentage differences in ultimate loads between the strengthened specimens and the unstrengthened specimens are also presented. The increase in ultimate load was approximately 31÷37% for the T2 specimens, which were already equipped with a diagonal bar prior to strengthening, whereas it reached about 62% for the T1 specimen, whose as-built reinforcement layout consisted only of horizontal and vertical steel bars.

3.3. *Analytical evaluation of the load capacity of strengthened specimens*

The load capacity of the strengthened specimens was also evaluated using analytical strut-and-tie (S&T) models developed in [42], which assume that the tensile force in the reinforcing bars is equal to the minimum of the bar yielding force and the bond-slip resistance force. Furthermore, the reliability of the proposed analytical approach requires verification not only of the strength and equilibrium of the strut-and-tie model, but also of the concrete compressive strength, as well as the equilibrium and load-carrying capacity of the nodes [42]. The contribution of the strengthening bar can be directly accounted for in the strut-and-tie (S&T) model developed for the unstrengthened specimen. If the strengthening bar is mechanically anchored at the bottom of the beam, its contribution to the load capacity of the dapped end can be assessed using the strut-and-tie (S&T) model shown in Fig. 19a, as suggested in Eurocode 2 [43]. However, mechanical anchorage of the diagonal bar is often impractical due to the presence of the bottom longitudinal reinforcement, which prevents drilling through the beam to the bottom, so the post-installed bar can only be bonded to the concrete, as in the present study. In this case, the increase in the ultimate load can be evaluated using the truss model shown in Fig. 19b, where the truss geometry, particularly the inclination of the strut within the full-depth beam section, is governed by the anchorage length of the strengthening bar [44]. Differently from the truss model of Fig. 19a, it is

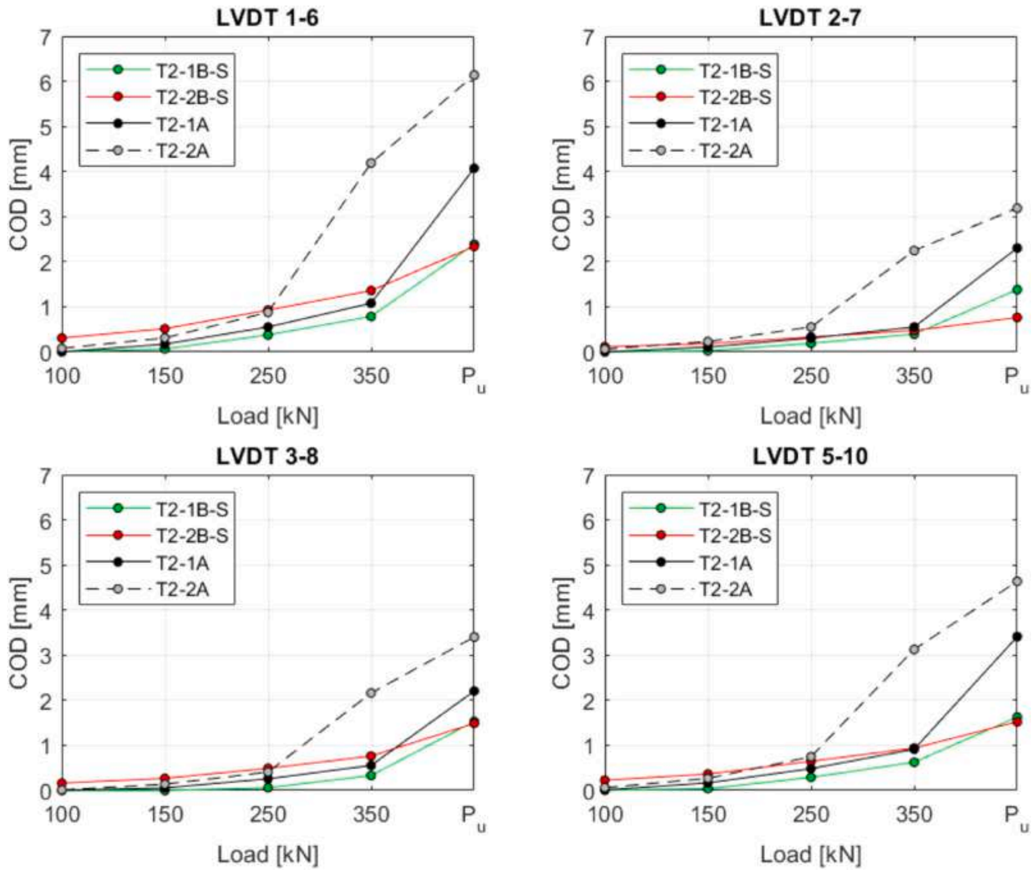

Fig. 11. Average crack opening displacements measured by all LVDTs as a function of the applied load (P) [kN] for the strengthened specimens (T2−2B-S and T2−1B-S) and the unstrengthened specimens (T2–1A and T2−2A).

evident that this truss model can develop only if horizontal reinforcement in the nib and hanger vertical reinforcement is provided to ensure static equilibrium and carry the associated axial forces.

3.3.1. *Analytical model for the strengthened T1 specimen*

For the strengthened specimen T1–1B, the load capacity is evaluated by summing the contributions of the as-built horizontal and vertical reinforcement, and the strengthening bar.

The horizontal bar in the nib and the hanger bars are considered within a truss model identified through an iterative approach, as described in [42], hereafter referred to as Truss A. The iterative calculation consists of progressively adding stirrups - whose maximum tie force is limited by their yield strength - to the resisting mechanism, starting from the one closest to the corner, until yielding of the horizontal bar or crushing of the concrete occurs. In this case, the calculation indicates that the first three stirrups are involved in the resisting mechanism, with the first two yielding and the third remaining in the elastic range. The maximum resisting load, equal to 402.7 kN, is reached when the horizontal reinforcement in the nib yields (Fig. 20).

The contribution to the load capacity of the diagonal strengthening bar, bonded to the concrete at its bottom end, could be evaluated using the strut-and-tie (S&T) model shown in Fig. 19b, nevertheless this model requires additional vertical reinforcement and horizontal reinforcement in the nib beyond that already involved in Truss A. The increase in the load capacity due to the post-installed bar is then considered using a sectional approach [42,45]: the increase in the ultimate reaction at the support is taken as the minimum of the ultimate shear strength (F) at section S (Fig. 21a) and the vertical component of the ultimate eccentric tensile axial force (N) at section S_1, inclined at 45°. In turn the ultimate axial force N is determined by the intersection between the moment–axial force interaction curve of section S_1 and the line describing the relationship between bending moment and axial force, $M=N \cdot d_g$, where the slope of the line is equal to the eccentricity d_g (Fig. 21a).

For specimen T1–1B, N is equal to 77.5 kN (Fig. 21) consequently, the maximum reaction under the nib holds 109.5 kN [= 77.5 / sin (45°)], which corresponds to an ultimate load of 173 kN. By summing the ultimate loads provided by the Truss A and the sectional approach, a total ultimate load of 402.7 kN + 173 kN = 575.7 kN is obtained. It is worth noting that those values are calculated using the yielding strength of reinforcements.

3.3.2. *Analytical model for the strengthened T2 specimens*

For specimens already equipped with diagonal reinforcement before strengthening (type T2), the contribution of the hanger reinforcement was evaluated using the Truss A [43] and the contribution of the diagonal bars with the Truss B shown in Fig. 22. In the Truss A, at the yielding of the horizontal bar in the nib, only the first two 14 mm hanger bars are activated in the resisting mechanism, remaining in the elastic field; a maximum load of 126.8 kN is reached. The horizontal component of the compression strut is equilibrated by the 14 mm C-shaped bars. The contribution of the diagonal bars, represented by Truss B, results in an external load of 242.7 kN.

The contribution of the diagonal strengthening bar can be taken into account by using the sectional approach as in the previous case (Fig. 21). However, in contrast to the aforementioned configuration, its influence on the ultimate load is reduced due to slippage of the longitudinal reinforcement, which is attributed to the absence of a longitudinal bar anchorage plate (Fig. 1). Indeed, the addition of the strengthening bar increases the maximum load capacity and the corresponding bending moment, so inducing higher tensile forces in the longitudinal bottom reinforcement.

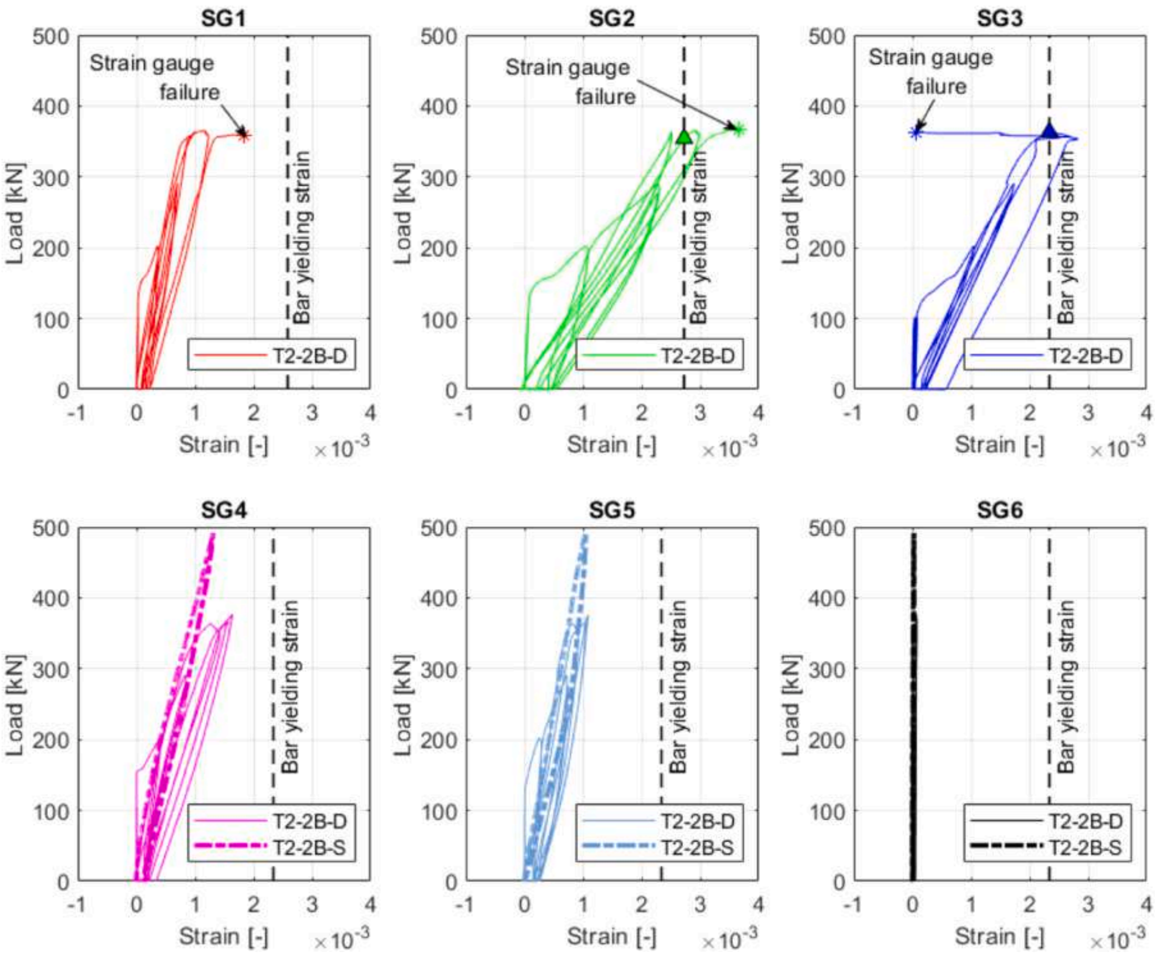

Fig. 12. Strain gauge results for the tests T2−2B-D and T2–2B-S.

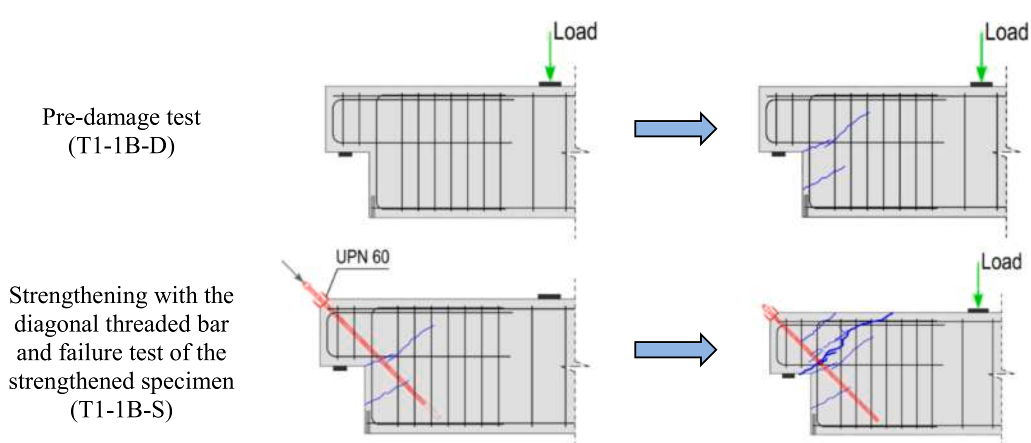

Fig. 13. Test phases of the specimen T1−1B.

Starting from the reaction R obtained through the sectional analysis ($R = 109.5$ kN), attention is focused on the critical section corresponding to the onset of slippage of the bottom reinforcement (section A-A in Fig. 23). At this section, the bending moment is M= 109.5·0.722 = 79.09 kNm, which induces a tensile force of 164.13 kN in the horizontal bottom bars (Fig. 23).

At failure, an engineering approximation of the tensile force in the bottom horizontal reinforcement at section A-A is obtained assuming that the ultimate capacities of the three distinct resisting mechanisms (Truss A, Truss B and the sectional mechanism) can be superimposed. Since the bottom reinforcement is subjected to tensile forces of 150.7 kN and 330.7 kN at the failure of Truss A and Truss B, respectively, and to a tensile force of 164.13 kN at the failure of the sectional mechanism, the superposition assumption yields a total tensile force of 645.6 kN. The corresponding load capacity of type T2 specimens is 542.5 kN, obtained by summing the individual contributions of each mechanism: 126.8 kN from Truss A, 242.7 kN from Truss B, and 173 kN from the sectional mechanism. This value exceeds the experimentally observed ultimate

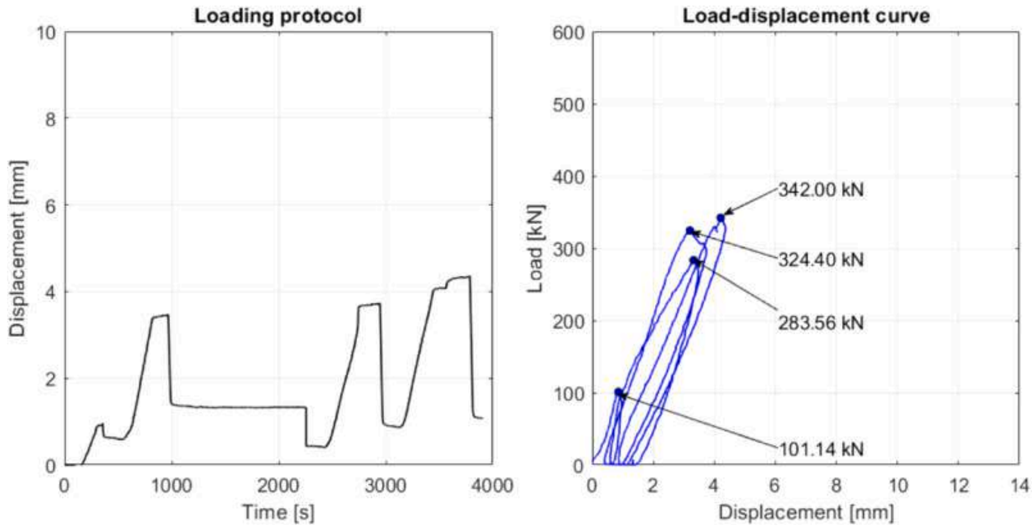

Fig. 14. Loading protocol and load-displacement curve for the pre-damage test T1−1B-D.

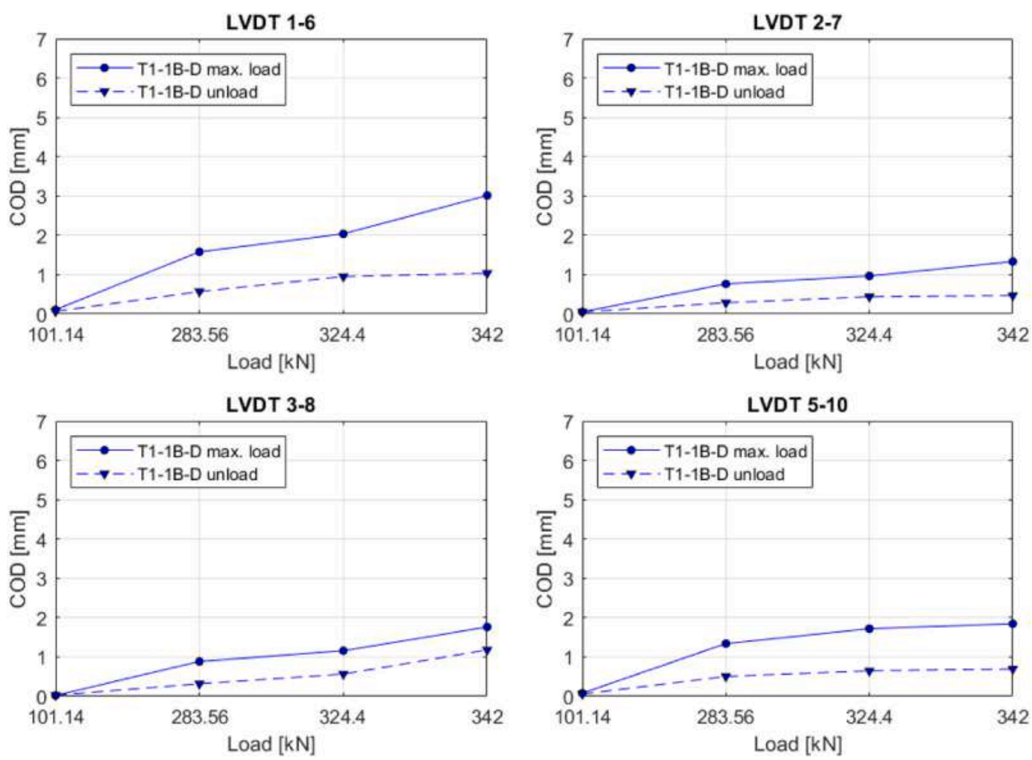

Fig. 15. Average crack opening displacements measured by all LVDTs as a function of the applied load (P) [kN] for the pre-damage test T1−1B-D.

loads of 491 kN (specimen T2–2B) and 512 kN (specimen T2–1B), indicating that, due to slippage of the bottom reinforcement, the average experimental capacity (≈ 500 kN) is approximately 8% lower than the predicted value. The tensile force at which slippage of the bottom bars occurs can be estimated by applying the same reduction factor (0.08), giving 0.92 × 645.6 ≅ 594 kN, while the anchorage length can be obtained from the experimental cracking pattern as about $L_a = 600$ mm (Fig. 23). Finally, considering the total bond perimeter of the four 24 mm diameter bars, the force of 594 kN corresponds to a bond strength $\tau = 3.28$ N/mm^2, close to the bond strength value provided by UK Code CS 455 (τ=3.52 N/mm^2, assuming the partial safety factor for bond equal to 1.0) [46], already utilized by Desnerck [47].

For the specimens without the strenthening bar, the maximum tensile force can be estimated as the sum of the forces at failure of Truss A and Truss B (481.4 kN), corresponding to a bond stress of 2.65 N/mm^2, lower than the bond stength, which explain the absence of slippage in the longitudinal bottom bars in the unstrengthened specimen [35] .

4. Discussion

The experimental campaign aimed to assess the effectiveness of post-installed diagonal steel bars as a strengthening technique for both undamaged and pre-damaged RC dapped ends.

A primary finding is the substantial increase in the load-carrying capacity observed in strengthened specimens. For the strengthened specimen without pre-damage (T2–1B-S), the strengthening led to an increase in the ultimate load capacity ranging from 34% to 39.6% compared to the unstrengthened specimens of the same type. In

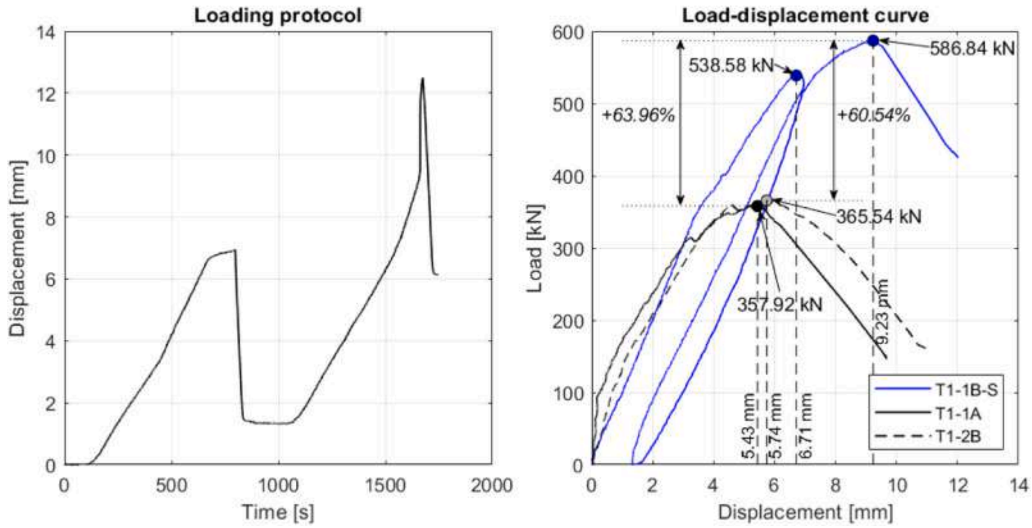

Fig. 16. Load-displacement curve of the tests T1−1B-S and comparison with tests on unstrengthened specimens T1−1A and T1−2B.

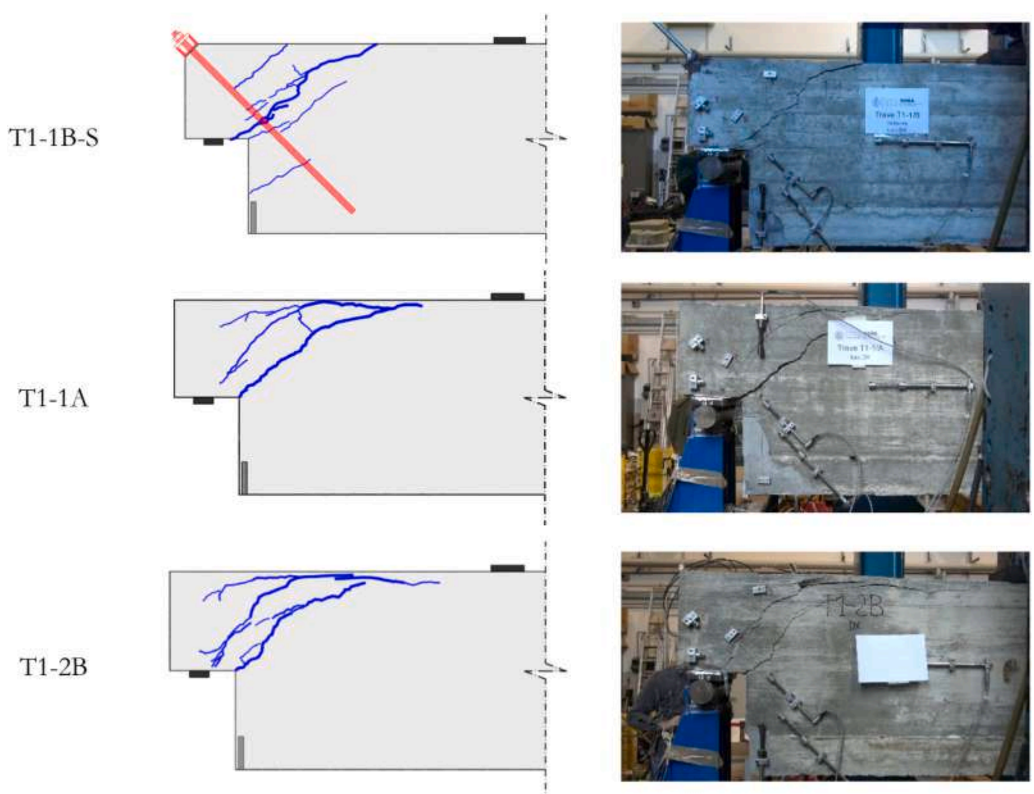

Fig. 17. Crack pattern at failure for tests T1−1B-S and T1−1B-R and comparison with tests on unstrengthened specimens T1−1A and T1−2B.

contrast, the specimen that was initially pre-damaged under load and then strengthened (T2–2B-S) showed an increase in load capacity between 28.3% and 34.1%. This suggests that the strengthening effectiveness in enhancing the load capacity of the pre-damaged specimen was only slightly lower than that of the specimen without pre-damage. The ability to enhance performance even after pre-damage due to overloading has significant implications for infrastructure rehabilitation strategies, potentially extending the lifespan of ageing bridges and reducing the need for costly and disruptive full replacements.

For the pre-damaged and strengthened specimen T1–1B, the increase in load capacity exceeded 60%, about twice the increase observed for the pre-damaged and strengthened specimen T2–2B. This result can be explained by the combination of the initial resisting mechanism, based solely on horizontal and vertical bars for specimens of the type T1, with the additional resisting mechanism activated by the presence of the strengthening diagonal bar.

Regarding ductility, the results indicate that the introduction of the strengthening bar, while significantly increasing the ultimate load capacity, led to a reduction in ductility. In particular, ductility evaluated according to [48] is about 2.3 for the unstrengthened T2 specimens, whereas values between 1.8 and 1.4 were obtained for the strengthened T2 specimens. For the T1 specimens, ductility values ranging from 1.7 to 2.0 were estimated for the unstrengthened configuration, while a value of approximately 1.6 was obtained for the strengthened specimen

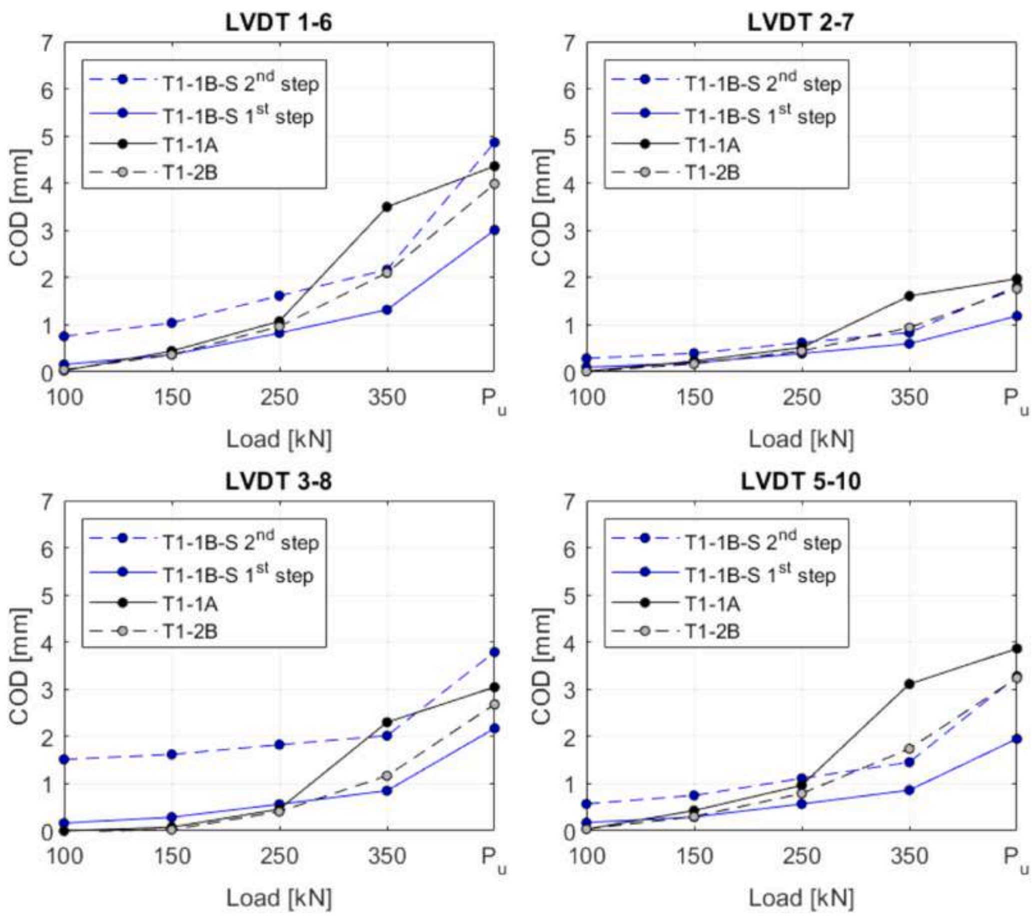

Fig. 18. Average crack opening displacements measured by all LVDTs as a function of the applied load (P) [kN] for the strengthened (T1−1B-S) and the unstrengthened specimens (T1−1A and T1−2B).

Table 1
Load-carrying capacity (in kN) registered in all tests.

Specimen	Failure load of the as-built unstrengthened specimen	Failure load of the strengthened specimen
T1–1B	362* [35]	586.84 (+62.11%)**
T2–1B	374* [35]	512.26 (+36.97%)**
T2–2B	374* [35]	491.42 (+31.40%)**

*Average ultimate load of tests on two unstrengthened specimens with the same reinforcement layout [35].
** Percentage increment compared to the average ultimate load of the unstrengthened specimens.

T1–1B-S. Nevertheless, considering the inherently brittle nature of dapped-end regions, the observed increase in load-carrying capacity can be regarded as more important for structural safety than the moderate reduction in ductility.

Unlike the unstrengthened specimens, where the failure mode was characterised by the formation and propagation of a dominant crack at the re-entrant corner of the nib, the strengthened specimens (e.g., T2–1B-S) showed a more distributed crack pattern. This change denotes a significant improvement in the structural reliability and safety, as it provides a greater warning before collapse. The effective control of crack opening displacements (COD) further supports this observation. As shown by the LVDT measurements, the strengthened specimens exhibited consistently lower COD values at various load stages compared to corresponding unstrengthened specimens, indicating enhanced stiffness and serviceability performance. The reduction in crack width is crucial for long-term durability, minimising the ingress of deleterious substances and extending the service life of the structure.

Although the results are promising, this study has some limitations that point the directions for future research. The bond behavior between the post-installed bars and the concrete was not directly tested. Future work should therefore include dedicated pull-out tests to evaluate the actual strength and anchorage of the system in both uncracked and cracked concrete. Moreover, the study considered only a single strengthening bar, and the proposed technique was evaluated for only two specific reinforcement layouts. Further research is needed to investigate the effects of different reinforcement ratios and alternative bar detailing. To support future experimental tests, detailed numerical modeling would also be very useful to better understand the interaction between the new and existing reinforcement.

5. Conclusions

This experimental investigation successfully evaluated the effectiveness of an innovative strengthening technique for RC half-joints using post-installed diagonal steel bars. The study provides

valuable insights into the mechanical behaviour of these critical components of bridges under enhanced conditions.

The key findings are summarised as follows:

- The proposed strengthening technique using a post-installed diagonal steel bar significantly increased the ultimate load-carrying capacity of RC half-joints. The ultimate load increased by 61% for specimens without diagonal bars (type T1) demonstrating its high efficiency in enhancing structural performance.
- The strengthening method proved to be highly effective also in increasing the load capacity of dapped ends, which have been pre-

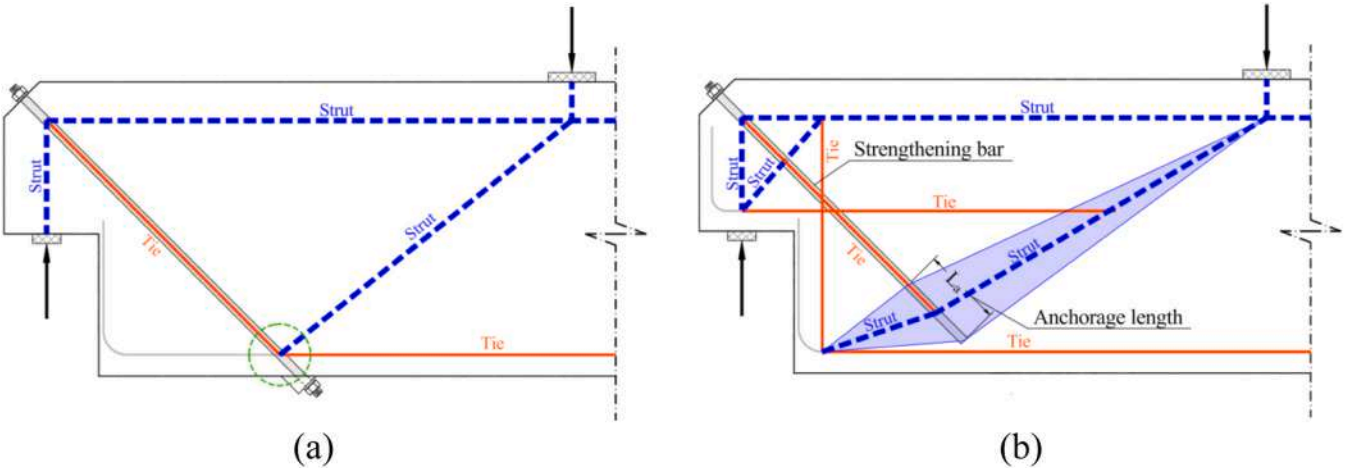

Fig. 19. S&T models for mechanically anchored (a) and bond anchored (b) post-installed bar.

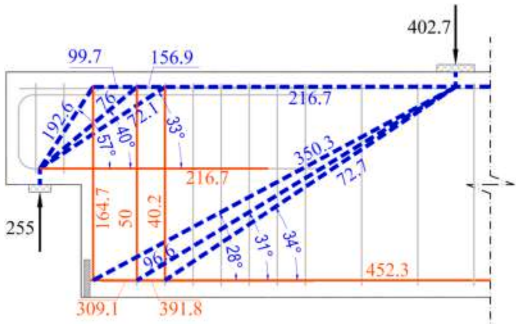

Fig. 20. S&T model for the T1 unstrengthened specimens (Truss A).

damaged under a load like the ultimate load of the unstrengthened specimen. The ultimate load increased by 34–40% for specimens with diagonal reinforcement (type T2) showing its potential as a viable repair solution for existing infrastructures.

The post-installation of the diagonal bar alters the failure mode of half-joints, as evidenced by a more distributed cracking pattern compared to the localized cracks observed in unstrengthened specimens. Additionally, the diagonal reinforcement improves crack width control (crack widths reduced by up to 60% at service load levels) which ultimately enhances the serviceability and safety of the structure.

In conclusion, the study highlights that the post-installation of internal diagonal steel bars represents a good solution for strengthening and repairing RC half-joints. Nevertheless, further investigation is needed to investigate bond behavior at the strengthineg bar-concrete interface, as well as the use of FRP materials for the strengthening bar and alternative strengthening layout. Such investigations could further enhance the reliability, durability and applicability of the proposed strengthening technique.

CRediT authorship contribution statement

Federico Gusella: Writing – original draft, Visualization, Software, Investigation, Formal analysis. **Giovanni Menichini:** Writing – original draft, Visualization, Software, Investigation, Formal analysis, Data curation. **Maurizio Orlando:** Writing – original draft, Validation, Supervision, Resources, Project administration, Methodology, Funding acquisition, Conceptualization. **Salvatore Giacomo Morano:** Writing – original draft, Validation, Supervision, Methodology, Conceptualization.

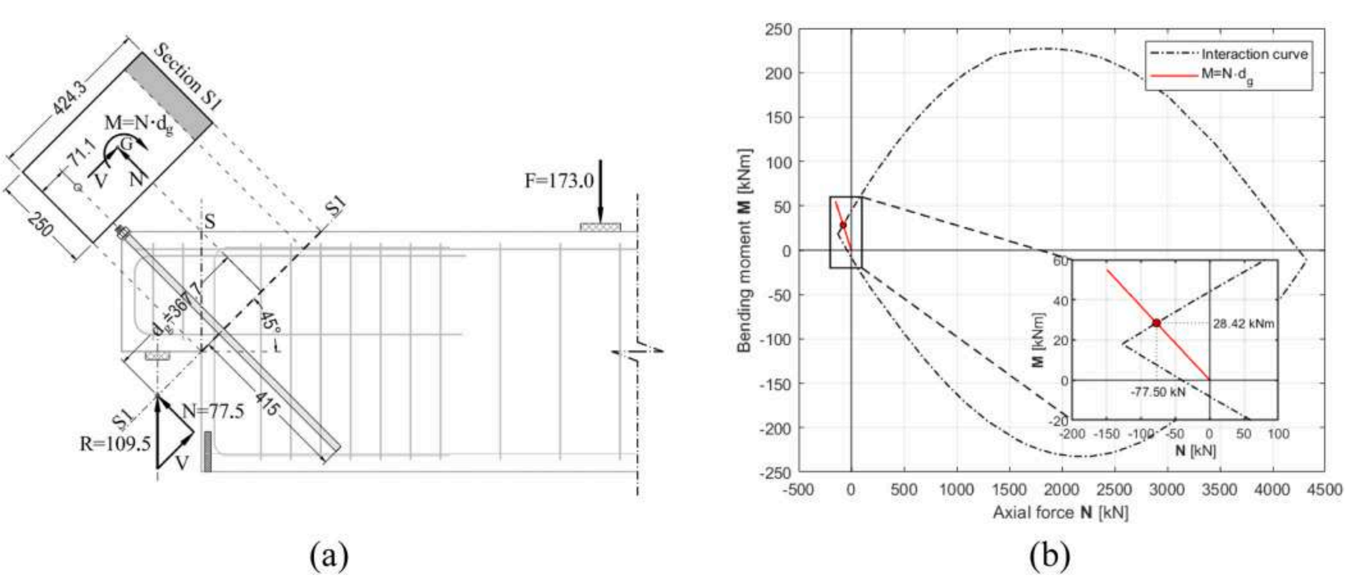

Fig. 21. Inclined section A-A identification (a) and section A-A moment-axial force interaction curve.

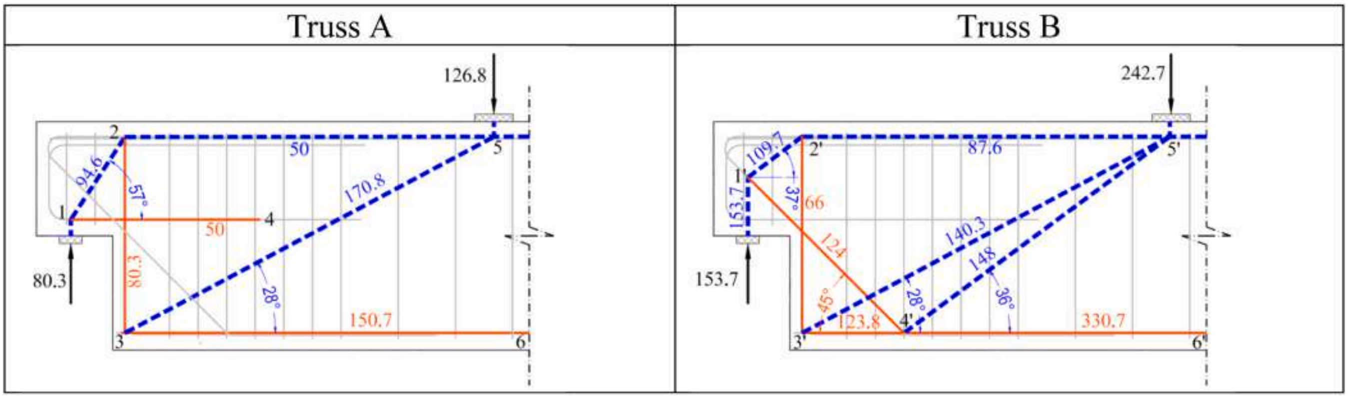

Fig. 22. S&T models for unstrengthened T2 type specimens.

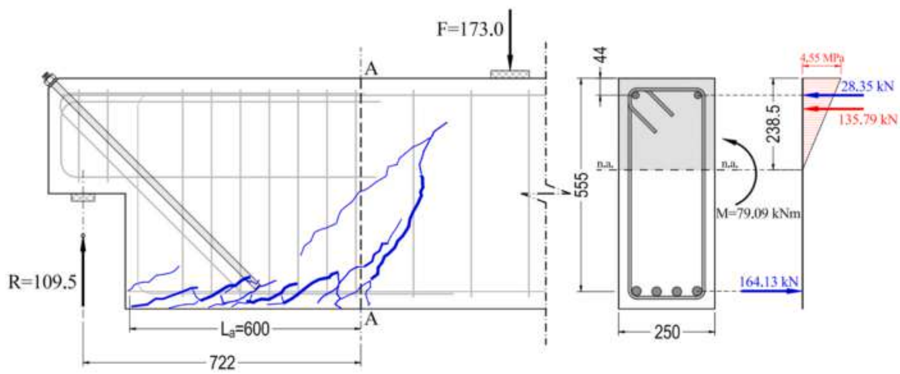

Fig. 23. Bending moment equilibrium at the section A-A.

Table 2
Experimental and analytical ultimate loads.

Specimen	Ultimate load of unstrengthened specimen		Ultimate load of strengthened specimen	
	Experimental [kN]	Analytical [kN]	Experimental [kN]	Analytical [kN]
T1–1B	362	402 (+11%) *	586	575.7 (−1.76%)*
T2–1B	374	369 (−1.34%)*	512	500** (−2.34%)*
T2–2B	374	369 (−1.34%)*	491	500** (1.83%)*

* Percentage differences between analytical and experimental load ($\frac{An - Exp}{Exp}$)

** Results obtained considering the slippage of the horizontal bottom bars.

Declaration of Competing Interest

The authors declare that they have no known competing financial interests or personal relationships that could have appeared to influence the work reported in this paper.

Acknowledgements

The study presented was conducted as part of the program of activities carried out within the agreement between the ReLUIS Interuniversity Consortium and the Superior Council of Public Works stipulated pursuant to art. 3 of the Decree of the Minister of Infrastructure no. 578 of 17 December 2020; however, this publication does not necessarily reflect the Council's position and assessments. The authors express their gratitude to the technicians of the Structures and Materials Testing Laboratory of the Department of Civil and Environmental Engineering in Florence, Enzo Barlacchi and Andrea Giachetti, for their support in the execution of tests. UNICAL SpA, particularly to Dr Marco Francini, is acknowledged for supplying the concrete used in casting the beams, and Mr. Claudio Attala for the preparation and installation of the strengthening bars.

Data availability

Data will be made available on request.

References

[1] Ministero delle Infrastrutture e dei Trasporti, Consiglio Superiore dei Lavori Pubblici. Guidelines for Risk Classification and Management, Safety Assessment, and Monitoring of Existing Bridges (in Italian). 2022.
[2] P.M. Johnson, A. Couture, R. Nicolet, Report of the Commission of inquiry into the collapse of a portion of the de la Concorde overpass, Gov. Que. (2007).
[3] M. di Prisco, M. Colombo, P. Martinelli, Structural aspects of the collapse of a RC half-joint bridge: case of the annone overpass, J. Bridg. Eng. 28 (2023) 5023007, https://doi.org/10.1061/JBENF2.BEENG-6063.
[4] G. Santarsiero, V. Picciano, A. Masi, Structural rehabilitation of half-joints in RC bridges: a state-of-the-art review, Struct. Infrastruct. Eng. (2023) 1–24, https://doi.org/10.1080/15732479.2023.2200759.
[5] S. Kun, R. Vogt, O. Leuenberger, Rehabilitation of reinforced concrete Gerber bridges, Proc. SMAR 2015 Third Conf. Smart Monit. Assess. Rehabil. Civ. Struct. (2015).
[6] S.G. Morano, The works of the rebirth of the Polcevera helical ramp in Genoa. calcestruzzo nella transizione. Ecol. Ecol. Transit., Gwmax editore, 2022, pp. 483–490.
[7] S. Hino, Y. Tahara, T. Tsutsumi, Strengthening for an existing RC Gerber bridge using external cables, IABSE Rep. Doi 10 (1999) 5169.
[8] Ruane K., Minehane M., O'Suilleabhain C. Rehabilitation of Haulbowline Bridges, Cork Harbour 2016.

[9] M.F. Granata, L. La Mendola, D. Messina, A. Recupero, Assessment and strengthening of reinforced concrete bridges with half-joint deterioration, Struct. Concr. 24 (2023) 269–287, https://doi.org/10.1002/suco.202200367.

[10] D.A. Smith, Refurbishment of the old Medway bridge, UK, Proc. Inst. Civ. Eng. - Bridg. Eng. 158 (2005) 129–139, https://doi.org/10.1680/bren.2005.158.3.129.

[11] F. Alessandrini, P. Burba, The structural degradation of supports (in Italian), Rass. Tec. Del. Friuli-Venezia-Giulia 4 (1994).

[12] M. Di Prisco, Critical infrastructures in Italy: State of the art, case studies, rational approaches to select the intervention priorities, Proc. fib Symp. 2019 Concr. Mater. Des. Struct. Int. Fed. Struct. Concr. (2019) 49–58.

[13] G. Santarsiero, V. Picciano, Post-tension retrofitting of RC dapped-end beams: A numerical investigation, Struct. Concr. 25 (2024) 3246–3264, https://doi.org/10.1002/suco.202300207.

[14] G. Cardinale, M. Orlando, Structural Evaluation and Strengthening of a Reinforced Concrete Bridge, J. Bridg. Eng. 9 (2004) 35–42, https://doi.org/10.1061/(ASCE)1084-0702(2004)9:1(35).

[15] A. Atta, M. Taman, Innovative method for strengthening dapped-end beams using an external prestressing technique, Mater. Struct. 49 (2016) 3005–3019, https://doi.org/10.1617/s11527-015-0701-8.

[16] Q.M. Shakir, R. Alliwe, Upgrading of Deficient Disturbed Regions in Precast RC beams with Near Surface Mounted (NSM) Steel Bars, J. Mater. Eng. Struct. « JMES » 7 (2) (2020).

[17] S.E.-D.F. Taher, Strengthening of critically designed girders with dapped ends, Proc. Inst. Civ. Eng. - Struct. Build. 158 (2005) 141–152, https://doi.org/10.1680/stbu.2005.158.2.141.

[18] G. Bertagnoli, M. Ferrara, L. Giordano, M. Malavisi, Preliminary Investigation on Steel Jacketing Retrofitting of Concrete Bridges Half-Joints, Appl. Sci. 13 (2023), https://doi.org/10.3390/app13148181.

[19] Lafranconi L., Massone G., Pasqualato G., Deiana M. Analysis and rehabilitation of the Generale Franco Romano viaduct Verifica Strutturale e miglioramento sismico del viadotto Generale Franco Romano 2016.

[20] K.-D. Peng, J.-Q. Huang, B.-T. Huang, L.-Y. Xu, J.-G. Dai, Shear strengthening of reinforced concrete beams using geopolymer-bonded small-diameter FRP bars, Compos. Struct. 305 (2023) 116513, https://doi.org/10.1016/j.compstruct.2022.116513.

[21] S.-Z. Liu, Y.-L. Bai, W.-H. Shi, S.-J. Mei, K.-D. Peng, Shear performance of engineering cementitious composite beams with longitudinal steel-FRP composite bars and glass FRP stirrups, J. Build. Eng. 125 (2026) 116223, https://doi.org/10.1016/j.jobe.2026.116223.

[22] T.P. Doğan, İ.H. Erkan, Ö. Anıl, R.T. Erdem, Strengthening of low performance reinforced concrete beam to column joints against seismic effects with textile reinforced mortar strips, J. Build. Eng. 120 (2026) 115442, https://doi.org/10.1016/j.jobe.2026.115442.

[23] T. Kaya, M. Aras, T. Yilmaz, Ö. Çalişkan, Ö. Anil, R.T. Erdem, Investigation of impact behavior of reinforced concrete beam to column connection strengthened with carbon fiber-reinforced polymer strips, Struct. Concr. 22 (2021) 1977–2010, https://doi.org/10.1002/suco.202000571.

[24] Ö. Mercimek, Ö. Anıl, S.T. Akkaya, R.T. Erdem, A. Çelik, Y. Kopraman, et al., Experimental behavior of shear deficient RC beams strengthened with CFRP strips against reversible cyclic earthquake load, Struct. Concr. 26 (2025) 6424–6447, https://doi.org/10.1002/suco.202401066.

[25] K.H. Tan, C.J. Burgoyne, Shear strengthening of dapped beams using FRP systems. FRPRCS-5 Fibre-reinforced Plast, 16–18. Reinf. Concr. Struct. Vol. 1 Proc. fifth Int. Conf. fibre-reinforced Plast. Reinf. Concr. Struct, Thomas Telford Publishing, Cambridge, UK, July 2001, pp. 249–258, 16–18.

[26] P.-C. Huang, A. Nanni, Dapped-End Strengthening of Full-Scale Prestressed Double Tee Beams with FRP Composites, Adv. Struct. Eng. - Adv. Struct. Eng. 9 (2006) 293–308, https://doi.org/10.1260/136943306776987010.

[27] T. Nagy-György, G. Sas, A.C. Dăescu, J.A.O. Barros, V. Stoian, Experimental and numerical assessment of the effectiveness of FRP-based strengthening configurations for dapped-end RC beams, Eng. Struct. 44 (2012) 291–303, https://doi.org/10.1016/j.engstruct.2012.06.006.

[28] A.I. Quadri, Behavior of disturbed region of RC precast beams upgraded with near surface mounted CFRP fiber, Asian J. Civ. Eng. 24 (2023) 1859–1873, https://doi.org/10.1007/s42107-023-00605-5.

[29] G. Sas, C. Dăescu, C. Popescu, T. Nagy-György, Numerical optimization of strengthening disturbed regions of dapped-end beams using NSM and EBR CFRP, Compos. Part. B Eng. 67 (2014) 381–390, https://doi.org/10.1016/j.compositesb.2014.07.013.

[30] Q.M. Shakir, B.B. Abd, Strengthening of self-consolidating high strength RC dapped ends with CFRP fabrics, J. Mater. Eng. Struct. «JMES» 6 (2019) 359–374.

[31] A. Abdelmoniem, H. Madkour, K. Farah, A. Abdullah, Numerical investigation for external strengthening of dapped-end beams, Scholars' Press, 2020.

[32] K. Flores Ferreira, M.C. Rampini, G. Zani, M. Colombo, M. di Prisco, Experimental investigation on the use of Fabric-Reinforced Cementitious Mortars for the retrofitting of reinforced concrete dapped-end beams, Struct. Concr. 24 (2023), https://doi.org/10.1002/suco.202200743.

[33] A.T. Baraghith, A.-H.A. Khalil, E.E. Etman, R.N. Behiry, Improving the shear behavior of RC dapped-end beams using precast strain-hardening cementitious composite (P-SHCC) plates, Structures 50 (2023) 978–997, https://doi.org/10.1016/j.istruc.2023.02.059.

[34] D. D'Angela, G. Magliulo, C. Di Salvatore, E. Cosenza, Computational modeling of reinforced concrete dapped-end beams, Comput. Civ. Infrastruct. Eng. 40 (2025) 1545–1576, https://doi.org/10.1111/mice.13390.

[35] G. Menichini, F. Gusella, S.G. Morano, M. Orlando, RC dapped-end beams with various reinforcement layouts: An experimental investigation, Eng. Struct. 322 (2025) 119043, https://doi.org/10.1016/j.engstruct.2024.119043.

[36] N. Spinella, D. Messina, Load-bearing capacity of Gerber saddles in existing bridge girders by different levels of numerical analysis, Struct. Concr. 24 (2023) 211–226, https://doi.org/10.1002/suco.202200279.

[37] Deutsches Institut für Bautechnik (DIBt). European Technical Assessment ETA-22/0001 V3: Fischer injection system FIS EM Plus. 2024.

[38] Y. Xu, W. Liang, X. Ding, Y. Wang, Experimental Investigation on the Effect of Wetting–Drying Cycles on Bond Performance of GFRP Adhesive Anchors in Concrete, Buildings 16 (2026) 1649, https://doi.org/10.3390/buildings16091649.

[39] EN 12390-3. Testing hardened concrete - Part 3: Compressive strength of test specimens 2019.

[40] EN 12390-6. Testing hardened concrete - Part 6: Tensile splitting strength of test specimens 2010.

[41] EN 12390-13. Testing hardened concrete - Part 13: Determination of secant modulus of elasticity in compression 2021.

[42] G. Menichini, F. Gusella, M. Orlando, Methods for evaluating the ultimate capacity of existing RC half-joints, Eng. Struct. 299 (2024) 117087, https://doi.org/10.1016/j.engstruct.2023.117087.

[43] EN 1992-1-1. Eurocode 2: Design of concrete structures. Part 1-1: General rules and, rules for buildings, European Committee for Standardization, Brussels, Belgium, 2004.

[44] P. Bamonte, P.G. Gambarova, R. Invernizzi, Bond role in strut-and-tie systems modelling reinforced-concrete members, Eng. Struct. 209 (2020) 109946, https://doi.org/10.1016/j.engstruct.2019.109946.

[45] Del Giudice G. Reinforced concrete bridge with dapped-end beams (in Italian). Vitali e Ghianda. Genova: 1967.

[46] Highways England, Transport Scotland, Welsh Government, Department for Infrastructure (Northern Ireland). CS 455: The assessment of concrete highway bridges and structures. 2022.

[47] P. Desnerck, J.M. Lees, C.T. Morley, Strut-and-tie models for deteriorated reinforced concrete half-joints, Eng. Struct. 161 (2018) 41–54, https://doi.org/10.1016/j.engstruct.2018.01.013.

[48] R. Park, Evaluation of ductility of structures and structural assemblages from laboratory testing, Bull. New. Zeal Soc. Earthq. Eng. 22 (1989) 155–166.